Unione europea
Fondo sociale europeo

REPUBBLICA ITALIANA

REGIONE AUTÒNOMA DE SARDIGNA
REGIONE AUTONOMA DELLA SARDEGNA

A.D. MDLXII

UNIVERSITÀ DEGLI STUDI DI SASSARI

International PhD School in Life Sciences and Biotechnologies

Curriculum: Biochemistry, Physiology and Molecular Biology
Coordinator: Prof. Leonardo Antonio Sechi

XXIX Ciclo

Glycosaminoglycans purification and characterization: from pathophysiology to tissue engineering.

Coordinator: **Prof. Leonardo Antonio Sechi**

Tutor: **Prof. ssa Marilena Formato**
Co-Tutor: **Prof. Lorenzo Moroni**

Maastricht University

PhD Student: **Dott.ssa Michela Idini**

uniss
UNIVERSITÀ DEGLI STUDI DI SASSARI

Michela Idini

Glycosaminoglycans purification and caracterization: from pathophysiology to tissue engineering.

PhD thesis in PhD school in Life Sciences and Biotechnologies,
Biochemistry, Physiology and Molecular Biology curriculum
Università degli studi di Sassari

TABLE OF CONTENT

ABSTRACT

Glycosaminoglycans (GAGs) are linear polysaccharide chains which, with the exception of Hyaluronan, are covalently linked to a core protein to assemble a more complex molecule called Proteoglycan (PG). GAGs/PGs are involved in several physiological and pathological processes being among the major constituents of the Extracellular Matrix. Regarding their role in the Peripheral Nervous System (PNS), GAGs/Proteoglycans-mediated interactions participate in proliferation, synaptogenesis, neural plasticity and regeneration. Generally PNS nerve fibers have a remarkable ability to regenerate, leading to an almost complete recovery of normal function and this process is governed by glial cells known as Schwann cells, by their unusual capacity to metamorphose into cells driving the healing process.

However, posttraumatic nerve repair continues to be a major challenge in restorative medicine and micro-surgery. Although progress has been made in surgical techniques, functional recovery after a severe lesion of a major nerve trunk is often incomplete and unsatisfactory.

In this PhD project I discuss the role of glycosamynoglycans in promoting the regeneration processes in Schwann Cells seeded in electrospun scaffolds functionalized with purified GAGs from porcine aorta tissue.

Results show that Schwann cells seeded in Polycaprolactone (PCL) scaffolds increase proliferation and metabolic activities per time points and the levels of protein expression vary in cells seeded in functionalized scaffolds.

1 INTRODUCTION

1.1 GLYCOSAMINOGLYCANS/PROTEOGLYCANS

GAGs are large linear polysaccharides consisting in repeating disaccharide units each composed of an amino sugar [N-acetylglucosamine (GlcNAc), or N-acetylgalactosamine (GalNAc)] and an uronic acid [glucuronic acid (GlcA) or iduronic acid (IdoA)] or galactose (1-3).

Based on the amino sugar of the disaccharide units, GAGs can be classified into two groups: galactosaminoglycans and glucosaminoglycans. Galactosaminoglycans include chondroitin sulfate (CS), dermatan sulfate (DS), whereas glucosaminoglycans consist of hyaluronic acid (HA, also called hyaluronan), heparan sulfate (HS), Heparin (HE), and keratan sulfate (KS).

The constituent disaccharides are GlcA and GlcNAc for HA, GlcA and GalNAc for CS, IdoA and GalNAc for DS, GlcA or IdoA and GlcNAc for HS, and galactose and GlcNAc for KS (Fig. 1).

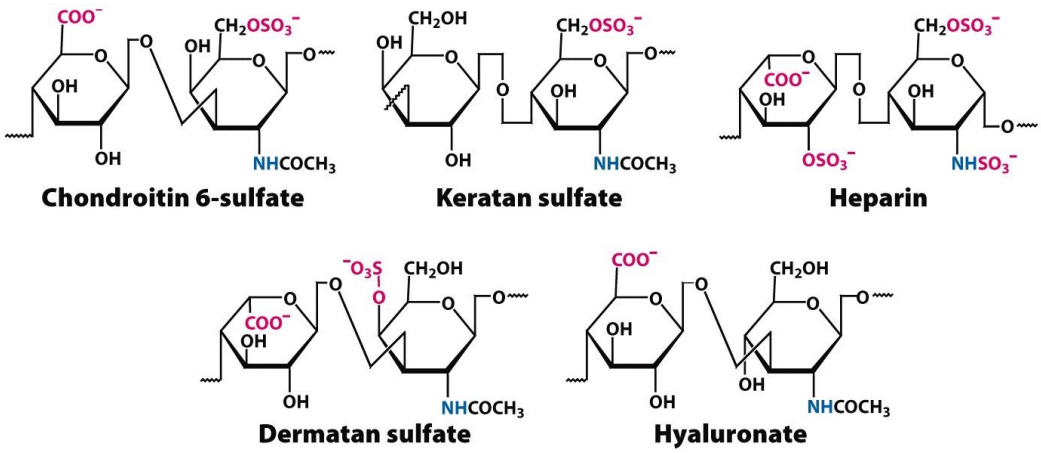

Figure 1. Glycosaminoglycans disaccharide units.

DS is also known as CS-B because it is a modified form of CS, whereas Heparin is a special form of HS present in mast cells. Heparin is made exclusively as serglycin proteoglycan, is highly sulfated, and contains more IdoA residues than does HS. HA lacks of sulfate groups and is not attached to a core protein, whereas other GAGs contain sulfate groups at various positions and are always attached to a core protein.

Proteoglycans represent a large group of glycoproteins that are ubiquitously present in the ECM or on the cell surface of virtually all animal cells (Fig. 2) (2, 4-6).

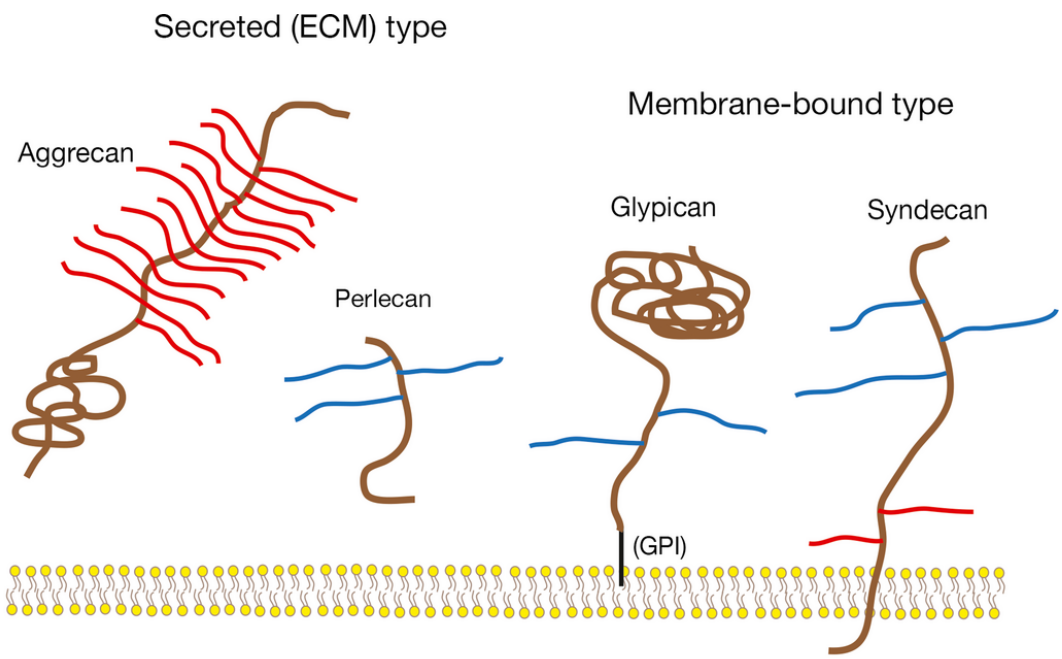

Figure 2. The proteoglycans consist of a core protein and covalently attached glycosaminoglycan (GAG)s. They can also be categorized into the ECM type and the membrane-bound type. Brown, red, and blue lines denote core proteins, CS, and HS, respectively.

They consist of core proteins and one or more covalently attached GAG chains. Some proteoglycans contain only one GAG chain, whereas others

have more than 100 GAG chains. The attachment site is a Ser residue in the core protein, and generally contains the -Ser-Gly-X-Gly- sequence, in which X can be any amino acid other than proline. Most proteoglycans contain O- and N-glycans in addition to GAGs, but GAGs are much larger and more abundant than other types of glycans, conferring the characteristic chemical properties of proteoglycans. Proteoglycans are named after their core proteins (for example, aggrecan, versican, glypican, and syndecan) and after their GAG chains (for example, CSPG and HSPG). They are also classified into ECM and membrane-bound types (Fig. 2).

Proteoglycans show a wide range of biological activities through their interaction with various molecules (2, 3, 5, 6). For example, CSPGs in cartilage interact with many ECM proteins (collagens, elastins, fibronectin, laminins, tenascins, and so forth), thereby providing the physical properties of cartilage, strength and elasticity, owing to their capacity to anchor fibrous proteins and to bind water and hydrated matrices. In addition to such relatively static roles, accumulating evidence has revealed that proteoglycans dynamically regulate intercellular signaling. Proteoglycans in the ECM bind morphogens, growth factors, and axon guidance molecules and protect them from proteolytic degradation. Proteoglycans thus act as a reservoir of signaling molecules and release them upon selective degradation of the ECM components, although the molecular mechanisms remain to be elucidated. Proteoglycans play critical roles in the formation of morphogen gradients, which are essential for development. Membrane-bound proteoglycans can act as receptors or co-receptors for signaling molecules and are essential for cell differentiation, growth, migration, and axon guidance. These functions of proteoglycans depend on the presence of GAGs and their diverse structures because the molecular interaction with signaling molecules is mediated by

GAGs.

Ones of the most studied proteoglycan families are Syndecans.

Syndecans are a gene family of four transmembrane heparan sulfate proteoglycans that bind, via their HS chains, various components of the cellular microenvironment.

Syndecan-1, the most extensively studied integral membrane HSPG, is abundant in epithelial cells and embryonic mesenchyme and can bind, via its heparansulfate chains, a wide variety of matrix molecules and growth factors such as collagens I, III, V, fibronectin, and fibroblast growth factors (FGF-2) (7-11). Furthermore, the proteoglycan core protein appears to associate intracellularly with F-actin, thus bridging the extracellular matrix with the cytoskeleton.

Syndecan-1 expression is regulated at multiple levels. Transcriptional control has been observed in vivo during development at sites of epithelial-mesenchymal interactions (12). In addition, syndecan-1 expression is regulated posttranscriptionally (12-14) and posttranslationally (15). These multiple levels of regulation precisely control the expression of syndecan-1 during various developmental processes, beginning as early as the four-cell stage (16) as well as during cutaneous wound repair (17). The shedding of the extracellular domain of syndecan-1 from the cell surface as an intact proteoglycan provides an additional potential control.

Syndecan-1 mRNA is abundant in fibroblastic and epithelial cells, being especially high in keratinocytes, but very low in endothelial and neural cells. This fits with its expression in adult tissues, where syndecan-1 mRNA is most abundant in tissues rich in epithelial cells and fibroblasts, such as skin, liver,

kidney, and lung, less abundant in brain and small intestine, and undetectable in cardiac and skeletal muscles (18).

Syndecan-2 is the major form in mesenchymal cells, and is present in neural tissue along with syndecan-3.

More than one syndecan is commonly present in a single cell type, but syndecan-4 is distinct in that it is present in a wide range of cells that form stable adhesions. Syndecan-4 is also the only mammalian family member that is consistently present in focal adhesions in colocalization with integrin, a transmembrane receptor involved in cell-cell and cell-matrix interactions (19).

Syndecan-4 mRNA is abundant in both epithelial and fibroblastic cells with intermediate levels in neural cells and lower amounts in endothelial cells. In tissues, it is abundant in liver and kidney, intermediate in amount in brain and lung, and low in heart, skeletal muscle, skin, and small intestine.

1. 2 PERIPHERAL NERVOUSE SYSTEM

The Peripheral Nervous System (PNS) is one of the two major components of the body's nervous system. In conjunction with the Central Nervous System (CNS), the PNS coordinates action and responses by sending signals from one part of the body to another. The CNS includes the brain, brain stem, and spinal cord, while the PNS includes all other sensory neurons, clusters of neurons called ganglia, and connector neurons that link to the CNS and other neurons.

1. 2. 1 ANATOMY AND PHYSYOLOGY

Depending on the composition of the fibers peripheral nerves are classified in three main categories: sensory, motor and mixed nerves (20).

Sensory nerve fibers originate from pseudounipolar neurons located in the sensory ganglia (except VII cranial nerve and the mesencephalic root of the V cranial nerve).

On the other hand, motor nerve fibers originate from somatic and autonomic motor neurons located in the CNS.

While somatic or motor fibers directly reach the target skeletal muscle fibers, autonomic motor fibers create synapses in an ortho- or parasympathetic ganglion where the second order autonomic neuron is located, and the axon of which eventually reaches the target visceral organs (20).

Generally, the peripheral nerve is represented by a nerve fiber made by axons and the surrounding Schwann cells, but in reality nerves are composed of more than just nervous tissue. They have connective tissues implicated in their structure, as well as blood vessels supplying the tissues with nourishment. The outer surface of a nerve is a surrounding layer of fibrous connective tissue called **epineurium**. Within the nerve, axons are further bundled into **fascicles**, which are each surrounded by their own layer of fibrous connective tissue called **perineurium**. Finally, individual axons are surrounded by loose connective tissue called **endoneurium**. These three layers are similar to the connective tissue sheaths for muscles. Nerves are associated with the region of the CNS to which they are connected, either as

cranial nerves connected to the brain or spinal nerves connected to the spinal cord.

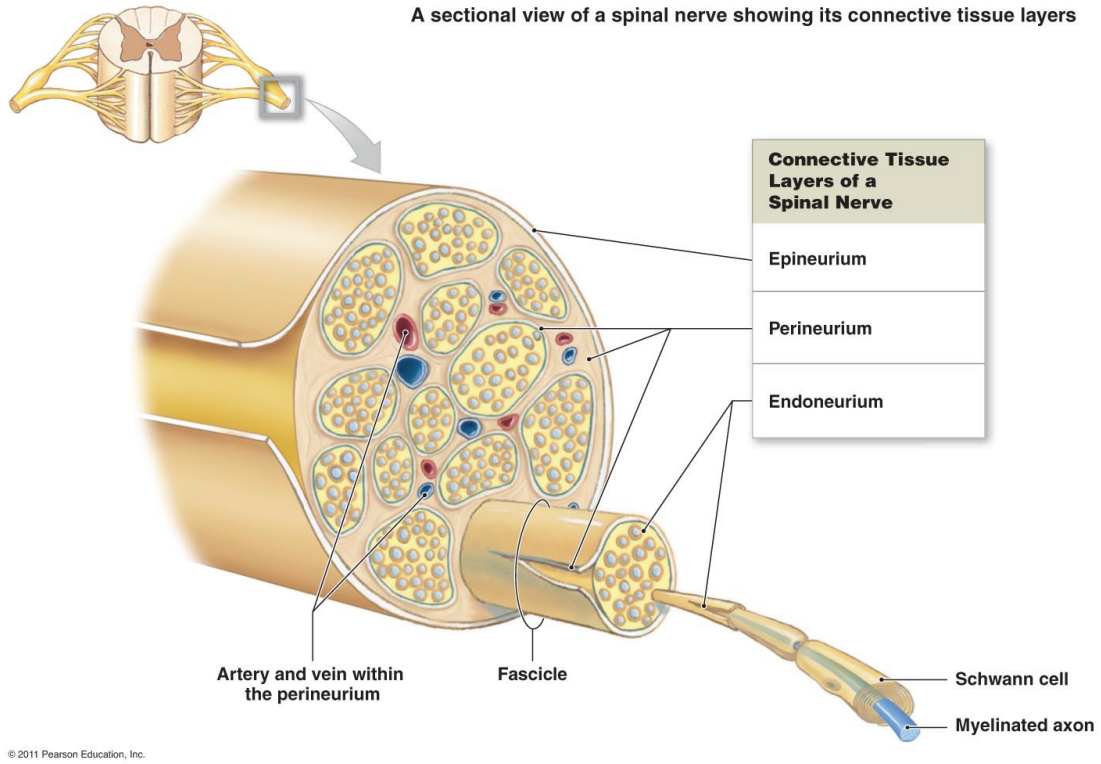

Figure 3. Structural components of peripheral nerves

Within the endoneurium, all axons are intimately associated with Schwann cells. As shown in Figure 3, the myelin of each myelinated axon is formed from the plasma membrane of a Schwann cell wrapped tightly multiple times around the axon. Thus, a single Schwann cell envelops a single myelinated axon, forming an internode. Along a myelinated axon, the points of separation between myelinating Schwann cells in series are called *nodes of Ranvier*. Unmyelinated axons are enveloped by Schwann cell cytoplasm and plasma membrane but do not have multiple wrappings of Schwann cell plasma membrane. A single Schwann cell may envelop several unmyelinated axons. The Schwann cell of each myelinated axon or group of unmyelinated axons is surrounded by a basal lamina of type IV collagen, fibronectin,

laminin, and heparan sulfate proteoglycan (21). Between the axons this is a loose connective tissue constituting of type I and type II collagen fibrils in longitudinal orientation, fibroblasts, a few mast cells and macrophages, and endoneurial fluid.

The perineurium (Fig. 3) is formed by up to 15 layers of flat perineurial cells interspersed with layers of type I and type II collagen fibrils and elastic fibers in circumferential, oblique, and longitudinal orientations (22). Each layer of perineurial cells has a nearly complete basal lamina (21), and the very organized basal lamina of the innermost layer contains laminin, as well as heparan sulfate proteoglycan and fibronectin (23). Adjacent perineurial cells are linked by tight junctions, and the most internal perineurial cells form a perineurial diffusion barrier that functions with the blood-nerve barrier in controlling the endoneurial environment (24, 25). These layers of collagen and perineurial cells provide mechanical strength, making the perineurium the primary load bearing portion of the nerve (26-28).

Nerve fascicles are held together and surrounded by a connective tissue layer, termed the epineurium (Fig. 3). If the nerve contains more than one fascicle, the epineurium may be divided into epifascicular epineurium surrounding the entire nerve and interfascicular epineurium separating nerve fascicles. The epineurial layer includes bundles of type I and type III collagen fibrils and elastic fibers, as well as fibroblasts, mast cells, and fat cells. The number of fascicles and the proportion of epineurial connective tissue are variable between nerves and along the length of a single nerve (29). Axons do not remain in the same fascicle throughout their length (30). The interchange of axons between fascicles may help to minimize functional deficits following partial injury to the nerve (29), but also may result in a wide distribution of macrophages cleaning up the debris from axons undergoing Wallerian

degeneration after injury. Interfascicular epineurium is loosely attached to the perineurium, allowing for sliding of one fascicle independently of an adjacent fascicle (31). There is abundant epineurial connective tissue in nerves that contain many fascicles, and the connective tissue facilitates the dispersion of compressive forces (32).

The outermost tissue of the epineurium is attached to perineural fascial components of the connective tissue surrounding the epineurium (31), and the density and strength of the attachments differ along the length of a nerve. The perineural loose connective tissue may contain a significant amount of adipose tissue, which serves to protect the nerve at sites of recurrent compression and facilitates transverse and longitudinal gliding of the nerve within the nerve bed. The epineurium is more tightly adherent to the surrounding connective tissues where vessels enter or exit the nerve and where the nerve branches (31). Additionally, there are points at which a nerve may be firmly attached to an anatomical landmark, such as the attachment of the common peroneal nerve near the neck of the fibula.

The blood supply to nerves is provided by coiled segmental arteries that enter the epineurium periodically along the length of the nerve and form the vasa nervorum. Arteries divide into epineurial arterioles that form an anastomotic network running primarily longitudinally within the epifascicular epineurium and the interfascicular epineurium. Epineurial arterioles are supplied with a perivascular plexus of serotoninergic, adrenergic, and peptidergic nerves (33, 34). Perforating arterioles cross the perineurium at oblique angles and carry a short sleeve of perineurial cells into the fascicle (21, 35). Perineurial arterioles have poorly developed smooth muscle and thus have limited ability to regulate intrafascicular blood flow (36). Within the endoneurium, arterioles immediately turn into large-diameter,

longitudinally oriented capillaries that allow blood flow in either direction (37). The endothelial cells of endoneurial capillaries are connected by tight junctions, thus forming the tight blood-nerve barrier (25). Venules return blood to the venous system. Of note, lymphatic capillaries are present only within the epineurium and there is no lymphatic drainage from the intrafascicular or endoneurial space .

1. 2. 2 NERVE REGENERATION

Trauma to peripheral nerve trunks may result in various extents of nerve fiber injury. The axonal fate is a critical factor in determining the extent, time course, and recovery following nerve injury.

After a peripheral nerve sustains a traumatic injury, complex pathophysiologic changes, including morphologic and metabolic changes, occur at the injury site. These complex changes also occur in the nerve cell body, in the segments proximal and distal to the injury site, and in the distal endings of both muscle end-plates and sensory receptors. Changes in the nerve at the site of injury begin almost immediately. With crushing or transection of a nerve trunk, significant changes take place in normal morphology and tissue organization proximally and distally to the lesion (Fig. 4).

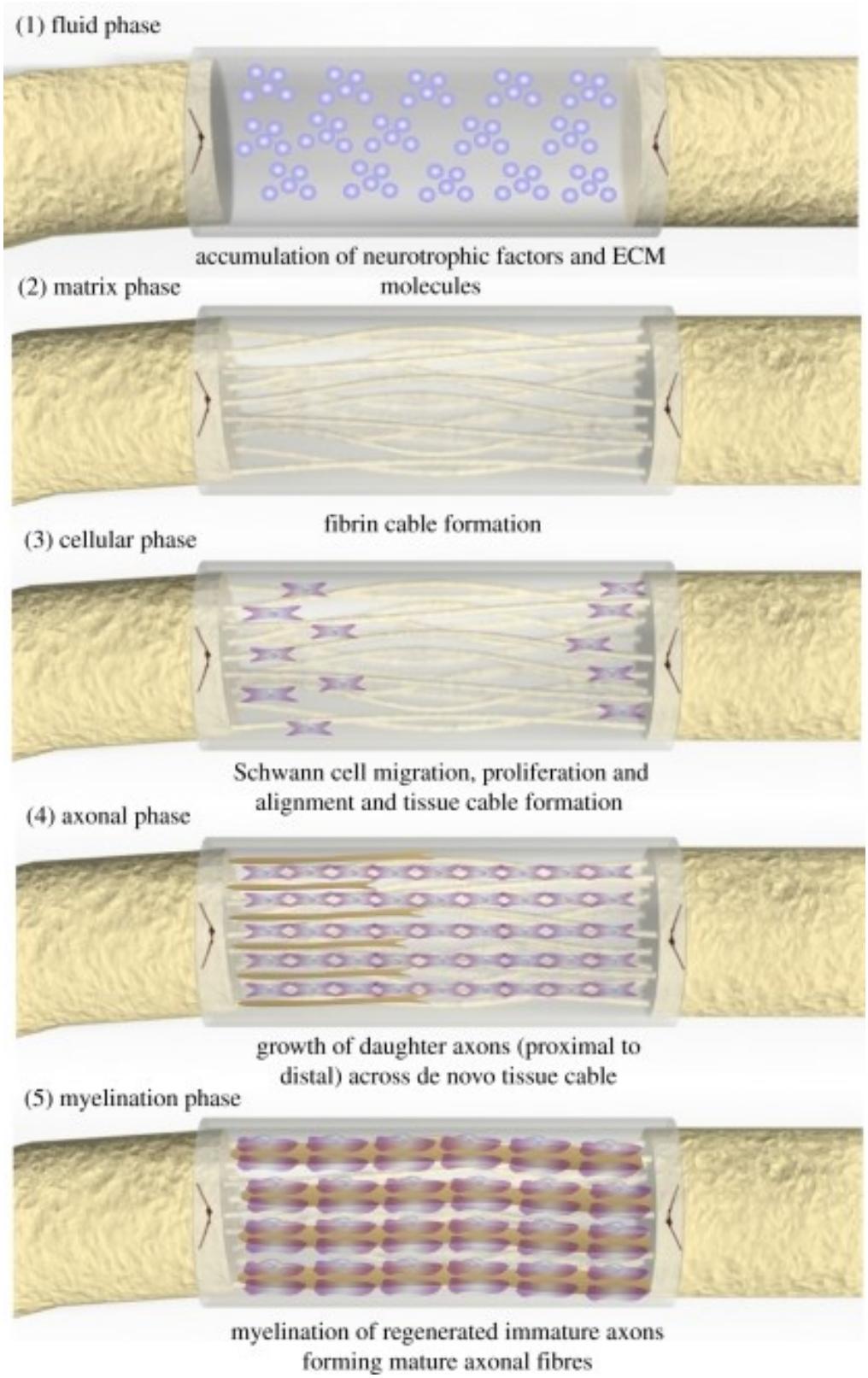

Figure 4. Nerve regeneration phases

EFFECTS IN THE PROXIMAL NERVE SEGMENT

Transection of an axon means amputation of a major part of the axoplasmic volume from the cell. It is therefore not surprising that such a traumatic event may lead not only to profound changes in cell body structure and function but also to cell death (38). These changes occur in both the dorsal root ganglia sensory neurons and in the motor neurons of the spinal cord anterior horn.

Changes can be seen in the nerve cell body as early as several hours after the injury. The series of morphologic changes that ensue in the cell body after injury are known as chromatolysis, and they entail cell body and nucleolar swelling, and nuclear eccentricity. All of these changes involve an alteration of the metabolic machinery from being primarily concerned with transmitting nerve impulses to fabricating structural components for reconstruction of the injured nerve (39, 40). The neurons switch from a ‘‘signaling mode’’ to a ‘‘growing mode’’ (41), and protein synthesis switches from neurotransmitter-related substances to those required for axonal reconstruction (42, 43). Metabolic changes include altered synthesis of many neuropeptides (44) and changes in synthesis of cytoskeletal proteins (45, 46) and growth-associated proteins (47, 48).

In the proximal segment, axons degenerate for some distance back from the site of injury, leaving the corresponding endoneurial tubes (the basal laminae of the Schwann cell) behind as empty cylinders. This retrograde degeneration may extend over one or several internodal segments, the length depending on the severity of the lesion.

Within hours after injury, the axon in the proximal segment produces a great number of collateral and terminal sprouts that advance distally along the

tube on the inside of the basal lamina (49, 50). The terminal sprouts arise from the tip of the remaining axon. Within hours of axotomy, small axoplasmic outgrowths have been observed from axoplasmic tips (51). This first wave of sprouts is followed by a second wave, appearing within the first 2 days (50, 52). Early sprouts can apparently degenerate before the definitive sprouting phase occurs. The time required for the definite sprouts to appear has been called the ‘‘initial delay’’ (53). A study on rat regenerating sciatic nerve (54) showed that sprouts have great variability in their behavior. There were ‘‘direct’’ projections (i.e., single sprouts crossing the gap), often traveling laterally in the interstump gap before entering a distal Schwann cell tube. ‘‘Arborizing’’ projections, in contrast, sampled 5–10 distal tubes from among more than 100 within their 50- to 100-mm spread. A single axon traveling within distal Schwann cell tubes continued to sprout collaterals, suggesting that the process of sprouting is a natural concomitant of regeneration. Schwann cell tubes in the distal segment were sometimes reinnervated by sprouts from several different parent axons.

Several researches show that Schwann cells play an important role in nerve regeneration at the site of injury. Schwann cells elaborate processes that include physical conduits that guide axons to their targets. The rate of axon regeneration is limited by the extension of these Schwann cell processes rather than by axonal growth (55). The regenerating units will initially lack myelin even when the parent axon is a myelinated fiber. With time, these unmyelinated fibers will become myelinated (56).

To reach the distal segment, the advancing sprouts have to pass a critical area between the proximal and distal stumps of the cut nerve: the interstump zone. The final success of the nerve regeneration is, to a great extent, dependent on what happens at this level and in what way local

chemical and cellular reaction can influence the growth of sprouts toward their peripheral pathways.

EFFECTS IN THE DISTAL NERVE SEGMENT

After nerve transection, the distal segment undergoes a slow process of degeneration known as Wallerian degeneration. This process starts immediately after injury and involves myelin breakdown and proliferation of Schwann cells. Schwann cells and macrophages are recruited to the injury site, and over a period of 3–6 weeks they phagocytize all the myelin and cellular debris.

Within hours after transection, the axon membrane fuses and seals the ends. Disintegration of the axons starts within the first days. The first stages of this process are characterized by a granular disintegration of axoplasmic microtubules and neurofilaments due to proteolysis (57-59).

The loss of axon–Schwann cell contact is a signal that causes the Schwann cell proliferation. Schwann cells upregulate the synthesis of several types of neurotrophic factors as Nerve Growth Factor (NGF) (60, 61). In addition to NGF, Schwann cells also produce and present various neurotrophins to the outgrowing axons (62) and the glial growth factor neuregulin (63). Proliferating Schwann cells organize themselves into columns (named bands of Büngner) and the regenerating axons associate with them by growing distally between their basal membranes.

The advancement of regenerating axons in the distal segment is promoted by neurite outgrowth-promoting factors, such as laminin and fibronectin (64-66). A number of cell adhesion molecules such as Neural cell adhesion

molecule (N-CAM), L1 cell adhesion molecule, the myelin-associated glycoprotein, and tumor-associated glycoprotein (TAG)-1, also play an important role (67, 68). In the distal segment, axon sprouts (which do not take an extraneural course) either approach a Schwann cell column or may grow at random into the connective tissue of the nerve. The Schwann cell columns are invaded by axon sprouts arising from parent axons in the proximal segment.

Since an excess number of sprouts invade the distal Schwann cell columns (69, 70), the initial number of axons present in the distal nerve segment may considerably exceed the number in the same nerve proximal to the lesion (71). With time, some of the regenerated axons, which have reached appropriate distal targets, enlarge, mature, and regain a close-to-normal diameter (70) as result of a trophic supply from the target organs. Other branches that do not reach the target are pruned away and disappear. After a few months of nerve regeneration, we will see a reorganization of the nerve trunk into a large number of miniature compartments, each surrounded by a new perineurium: a process in which the distal stump of a divided nerve became separated into numerous nerve bundles, or ‘‘minifascicles,’’ to replace the original large fascicle. This phenomenon is known as ‘‘compartmentation’’ (72). Initially, it occurs also in the proximal stump of a cut nerve and in the gap between the two ends as the axons advance. The stimulus to compartmentation is probably a disturbance of the endoneurial environment resulting from damage to the perineurium. The formation of numerous miniature fascicles expresses the need for restitution of the normal endoneurium environment around the nerve fibers as quickly as possible by restoring the perineurial barrier (73).

Prolonged denervation of the distal segment results in a progressive increase in collagen content and extensive changes in the distribution of collagen types have been observed in the endoneurium and perineurium (74). Collagen production in the endoneurium may result from fibroblast activity but it may also be a result of Schwann cell activity (75, 76).

When assessing the rate of axonal outgrowth in experimental animals, several factors seem to play a role, such as the nature of the lesion, the species and the method of assessment. The quality of outgrowth obtained after transection and suture is always worse than that obtained after a crush injury. The regeneration rate in rat and rabbit nerves falls within the range of 2.0–3.5 mm/day after transection and repair and 3.0–4.4 mm/day after a crush lesion (73).

1. 3 EXTRACELLULAR MATRIX COMPONENTS IN NERVE REGENERATION

The ECM is a physiological integrative matrix of complex molecular nature, where axons and supportive cells are immersed. The ECM is a three-dimensional network arranged in the intercellular space, which includes proteins and carbohydrates synthesized and secreted by the cells. It is present in the interstitial spaces of all tissues, playing important roles in cell migration, proliferation, and differentiation, and providing structural support and regulating intercellular communication. It contributes to mechanical tissue properties, allows the cells to form tissues, serving to cell communication, and forms paths where cells can move. In the peripheral nerve, the ECM is found in the basal lamina of Schwann cells and the endoneurium.

The basal lamina, produced by the Schwann cells, may be considered a layer of the ECM, mainly composed of collagen type IV, laminin, fibronectin, and nidogens (77-79). After injury, besides the degenerative process behold in the distal stump, basal lamina tubes remain as scaffolds where proliferative.

The ECM is composed of a complex network of secreted proteins, glyco-proteins, proteoglycans, and non-proteoglycan polysaccharides. The first group of components, the glycoproteins, can be classified into collagen and noncollagenous molecules.

Collagens are a superfamily of trimeric molecules composed of three identical triple helical chains that define tissue structures (80, 81). Up to 26 different types of collagens have been described, that are divided into different groups according to the structures they form. The main subfamilies are fibril-forming collagens (types I, II, III, V, XI), collagens banded-fibrils associated (IX, XVI, XIX, XXI, XXII), networking collagens (IV, VI, VIII, X), trans-membranous collagens (XIII, XXIII, XV), endostatin precursor collagens (XV, XVII), and other collagens. However, it is interesting to highlight the importance of collagen types related to fibril formation (collagen type I) and the basement membrane (collagen type IV).

Among the ECM noncollagenous molecules of glycoprotein origin, the most important are laminins and fibronectins.

Laminins are high-molecular weight proteins of the ECM, participating in cell differentiation, migration, and adhesion activities. They are an active part of the natural scaffolding which structure the tissues. They are mainly found in the basal lamina. Laminins are heterotrimers of α, β, and γ chains, and 18 different types have been described to date (82). The trimers are named

according to the composition of the different chain types, but usually it is the α chain that identifies the isoform. Secreted by Schwann cells, laminin-2 (α2, β1, γ1) and laminin 8 (α4, β1, γ1) are found in the peripheral nerves (83) whereas laminin 10 (α5, β1, γ1) can be detected in sensory end organs (84). Laminin is the adhesive component that gives the regenerative-promoting capability to basal lamina scaffolds after nerve injury (85) and has been shown to promote neuritogenesis in vitro (86).

Fibronectin is a noncollagenous glycoproteins of the ECM (87). It forms a fibrillar matrix similar to collagen and mediates cell-binding. Fibronectin is a dimer existing in different isoforms because of alternative splicing generation. Totally, 12 isoforms for mice and 20 for humans have been described. At first, soluble fibronectin is produced by hepatocytes, being found in the blood plasma. The insoluble form is incorporated into the membrane of many cells. In the nervous system, it is synthesized and secreted by Schwann cells and fibroblasts (78, 88). The important relations that it maintains with collagen type IV and laminins and with fibril formation make fibronectin an interesting candidate for scaffolding in nerve regeneration (80).

The ability of cells to interact with both laminins and fibronectins is mainly due to the expression of the cell adhesion molecule integrins in their membrane (89). Integrins are glycosilated heterodimers formed by α and β subunits. The integrin β1 subfamily is composed of integrins with a β1 subunit, which bounds to actin cytoskeleton, and the a subunit, which determines the specificity to the ECM molecule adhesion. Thus, integrin α1, α3, α6, and α7 can interact with laminin, whereas integrin α5 interacts with fibronectin. Expression of integrins on the growth cone determines the ability

of the growing axon to interact with the ECM. Moreover, laminin and fibronectin have the characteristic of binding to other ECM components. For instance, laminin interacts with nidogens, agrin, perlecan, fibulin-1, heparin, and sulfatides (90, 91), whereas fibronectin binds to collagen, fibrin, and heparan sulfate proteoglycans (92).

There are other noncollagenous glycoproteins of the ECM although they are probably not related to axonal regeneration after nerve injury. Nidogen-1 (also called entactin) forms noncovalent unions with laminin and collagen type IV and may play its role as a promigratory factor for adult Schwann cells (93). On the other hand, vitronectin binds to collagen and glycosaminoglycans (GAGs) (heparin), acting as a regulatory molecule controlling cell adhesion (94).

Fibrin is not associated with the mature tissue structure but it is a key factor in the repair strategy of the ECM components. It can form a provisional mesh after damage that will be later replaced by the mature components of the ECM secreted by invading cells. In the presence of thrombin, fibrinogen polymerizes into fibrin to form a dense meshwork of fibers (80, 95). In fact, formation of a fibrin cable between the two stumps when a gap nerve is repaired by a tube is needed to guarantee successful axonal regeneration.

1. 4 TISSUE ENGINEERING

Peripheral nerve injury is a large-scale problem annually affecting more than one million people worldwide. These injuries often result in painful neuropathies owing to reduction in motor function and sensory perception. Peripheral nerve injuries are common in both civil and military environments

and are primarily the result of transection injuries or burns, but may also arise from degenerative conditions (96, 97). Over relatively short nerve gaps, spontaneous natural regeneration may occur. However, over larger gaps, microsurgical repair is essential for nerve repair (98-100).

Conventionally, autologous grafts are gold standards and have been used to treat neural defects (101-103).

However, autografts have limitations that include short-age of nerves since it is taken from the patient. Moreover, there is a mismatch of donor-site nerve size with the recipient site, neuroma formation and lack of functional recovery (104, 105). Allogenic grafts, which are isolated from cadavers, are not limited by supply but suffer from host-graft immune rejection (106). To overcome immune rejection, several studies have been conducted to examine the potency of acellular nerve grafts (107, 108). However, as acellular nerve graft lacks viable cells, studies regarding nerve regeneration and remodeling of extracellular matrix are still in progress (108).

The use of pre-degenerated nerve grafts having high matrix metalloproteinase (MMP) expression shows some potential as it degrades the inhibitory chondroitin sulphate and proteoglycans thereby retaining the ability to promote nerve regeneration even in the absence of cells (108, 109).

Recent advances in nanotechnology (110) and tissue engineering (111, 112) have been found to cover a broad range of applications in regenerative medicine and offer the most effective strategy to repair neural defects. The major determinant in all tissue engineering research is to regulate the cell behavior and tissue progression through the development and design of synthetic extracellular matrix analogues of novel biomaterials to support three-dimensional cell culture and tissue regeneration. Ideal properties of a

scaffold for nerve regeneration are biocompatibility, low inflammatory potential, controlled biodegradability with non-toxic degradative products, porosity for vascularization and cell migration and three-dimensional matrices with appropriate mechanical properties to mimic the extracellular matrix (113-115).

Polymeric biomaterials are widely preferred as scaffolds for peripheral and central nerve regeneration both *in vitro* and *in vivo* (116-119). There is a wide choice of polymers available with programmable biodegradability, non-toxic/non-inflammatory nature, mechanical properties similar to the tissue to be replaced, high porosity that promotes cell attachment and growth, economical and simple manufacturing processes along with a potential for chemical modification leading to increased interaction with normal tissue (120). Several techniques such as nanofiber self-assembly, solvent casting and particulate leaching, gas foaming, emulsification/freeze-drying, liquid-liquid phase separation, electrospinning and computer aided design and manufacturing techniques have been employed to fabricate tissue engineering scaffolds with varying degrees of success (121-124).

2 AIM OF THE STUDY

The aim of this project was to study the interaction between Schwann cells and electrospun scaffolds functionalized with GAGs, purified from aorta porcine tissue, to mimic the extracellular matrix.

As mentioned previously, Schwann cells are the glial cells of PNS that lead the process of nerve regeneration by the secretion of trophic support molecules and the establishment of a supportive growth matrix.

To study the behavior of Schwann cells seeded in scaffolds, proliferation assays, metabolic activity assays and GAGs assays were performed. Immunofluorescence and western blot analysis were carried out using five different antibodies:

Syndecan 1 and **Syndecan 4**, transmembrane proteoglycans known to bind different proteins in ECM, like Fibronectin, Laminin and Collagen;

Integrin, a transmembrane receptor which forms focal adhesion in colocalization with Syndecan 4;

Laminin, to observe if Schwann cells can be able to produce ECM proteins;

and **p75**, also called neurotrophin receptor or low affinity NGF receptors, which is a marker of Schwann cells.

Understanding if GAGs can improve proliferative activities and binding capacities of the cells to the scaffolds could be promising to improve the process of nerve regeneration.

3 MATERIALS AND METHODS

3.1 PREPARATION OF ELECTROSPUN SCAFFOLDS

Electrospinning is a process that produces a film of fibers by pushing a liquid jet through a nozzle with an electric field (125-131). Fiber diameter can range from 2 nm to several micrometers by controlling the composition of the electrospinning solvent and the identity, degree of chain entanglements, and concentration of the starting polymer. Moreover, fiber alignment can be manipulated by controlling the motion of the collecting mandrel with respect to the source electrospinning suspension.

Electrospun Polycaprolactone (PCL) fiber mats used as fibrous scaffolds were fabricated by electrospinning from a 15% (w/v) PCL solution in 1:4 (v/v) Dimethylformamide (DMF) : chloroform. A blunt 20-gauge stainless steel hypodermic needle (o.d.) 0.8 mm was used as the nozzle. A polyurethane sheet and an aluminum foil wrapped around a rotating cylinder (cylinder size = o.d. 6 cm, length 19 cm) was used as the collector. The distance from the tip of the needle to the surface of the aluminum sheet (measured at a right angle to the surface) defining the collection distance was 14 cm. A High-Voltage power supply was used to generate a direct current potential of 20 kV. The emitting electrode of positive polarity was connected to the needle, while the grounding one was connected to the collector. The feed rate of the PCL solution was controlled by syringe pump at 1 mL/h.

The mandrel speed was regulate around 500 rpm (2.6 V) to obtain scaffolds with random fibers, and around 4000 rpm (9 V) to obtain scaffolds with

aligned fibers. The needle was set to move back and forth along the length of the cylinder to permit an homogeneous fibers deposition on top of the polyurethane sheet.

After continuous spinning for 15 minutes, homogenous PCL fibrous scaffolds were obtained. The morphology of the fibrous scaffolds and the size of the individual fiber segment therein were examined by a Philips XL30 scanning electron microscope. Multiple scanning electron microscopy (SEM) images were statistically analyzed using FIJI software, from which the mean value of the diameters of the fiber segments within the PCL fibrous scaffolds was determined.

3.2 GLICOSAMINOGLYCANS PURIFICATION

GAGs were purified as described by Naso et al. (132) and Cigliano et al. (133). In brief, porcine aortic root from 10-12-month-old pigs were obtained from a local slaughterhouse.

Fatty adherences were removed from aortic tissue by gentle peeling. Wet weight of each sample was determined after gently blotting with filter. Aortic minced tissues were dehydrated with 20 volumes of acetone at 4°C for 24 h, defatted with 20 volumes of chloroform: methanol (2 : 1, v/v) at 4°C for 24 h, dried for 24 h at 60◦C after centrifugation at 3300 ×g for 15 minutes, and finally weighed (dry-defatted tissue (DDT) weight). DDTs were rehydrated for 24 h at 4° C in 0.1 M sodium acetate, pH 5.8, containing 5 mM cysteine, and 5 mM ethylenediaminetetraacetic acid (EDTA) (37 volumes per gram of DDT).

Then, papain (0.3U/mg of DDT) was added to the mixture, which was incubated at 56° C for 48 h. The digestion was stopped by boiling the solution at 100°C for 5 min and then by centrifugation (9000 ×g for 15 min at 4◦ C).

Digest supernatant was loaded on a diethylaminoethyl (DEAE) Sephacel column (1.5 × 50 cm, 70 mL), equilibrated with 50 mM sodium acetate, pH 6.0. The column was then washed with the same buffer (until reaching Abs_{280} < 0.05) and eluted with a one-step salt gradient (1.5 M NaCl). Fractions of 5 mL were collected and assayed for hexuronate content by the method of Bitter and Muir, using glucuronolactone as a standard (134). Fractions containing GAGs were pooled and precipitated using 4 volumes of cold absolute ethanol. The mixture was left overnight at −20◦C, and the precipitate was separated by centrifugation, washed twice with ethanol, and then dried.

The total amount of GAGs was normalized to the fresh/DDT weight to estimate the tissue concentrations.

GAG composition was determined by discontinuous cellulose acetate electrophoresis (135). Alcian Blue stained strips were acquired (Gel Doc XR System) and analyzed using Quantity One 4.6.3 from BioRad Laboratories. Total mass of GAG was determined by reference to established GAG/uronic acid weight ratio.

3.3 ELECTROSPUN SCAFFOLDS FUNCTIONALIZATION

A common way of creating a covalent bond is by letting a carboxyl group react with a primary amine creating an amide bond, the same bond that links

amino acids together in a protein. *In vivo*, this reaction is brought about by the action of many enzymes and other molecules. *In vitro*, the use of coupling reagents is necessary. For example, the carboxyl group is converted to an ester by the use of N-(3-dimethylaminopropyl)-N'-ethylcarbodiimide hydrochloride (EDC). The ester can then react with the amine to form the amide bond. In order to increase the yield of this interaction, N-hydroxysuccinimide (NHS) is usually used together with EDC (Fig. 5). It reacts with the EDC-ester, protects it from hydrolysis and makes a better leaving group for the subsequent reaction. In this case, a surface modification via aminolysis of the polyester was followed by functionalization with GAGs. Aminolysis of a polyester surface is extremely advantageous as it requires only a single step to generate a functional surface. This way would explore the use of aminolysis as a one step method in generating functional polyesters from which to attach biologically active molecules.

A commonly used polymer for this aminolysis reaction is PCL because it has desirable biocompatibility and biodegradation. This polymer characterized by its hydrophobicity, for this reason the aim of the aminolysis reaction is to generate a more hydrophilic surface (through the introduction of polar amine groups) and increase the compatibility with proliferating cells.

The most common diamine used in the aminolysis of PCL is 1,6-hexamethylenediamine (HMDA).

In the present work PCL scaffolds were first aminolysed and then functionalised with GAGs (Fig. 5).

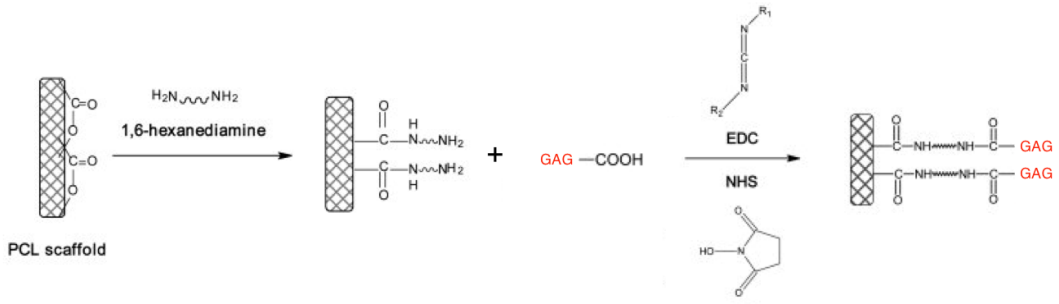

Figure 5. Aminolysis and functionalization reactions.

First of all, dried scaffolds were incubate 1 h at 37°C with 5% HMDA in isopropanol and then washed three times with water. GAGs purified from porcine aorta tissue (100 μg_{UA} solubilized in 100 µL H_2O) were added in each scaffolds. As negative control scaffolds no functionalized were used; in this case 100 µL of water without GAGs were added. A solution of 50 mM EDC/NHS in 2-(*N*-morpholino)ethanesulfonic acid (MES) was added in each scaffolds and left over night at room temperature.

Prior to seeding, no functionalized and functionalized scaffolds (o.d 15 mm) were placed into wells of a 24-well non-treated tissue culture plate (VWR). Each scaffold was pushed on the bottom of the well with O-rings (Alwin Höfert) to prevent cells from migrating out of the scaffolds onto the culture plate. Afterwards, supplemented (L- glutamine, FBS, penicillin-streptomycin) DMEM media was added in each well and incubated at 37°C with 5.0% CO_2 for 24 h.

To asses the level of GAG functionalization, an Alcian blue staining protocol was developed. In brief, scaffolds were placed in 24-well-plate and stained with Alcian blue solution (0.1% Alcian blue, 10 % EtOH, 0.1% CH_3COOH, 0.03 M MgCl2 0.03 M in water) for 30 min at room temperature. Then scaffolds

were washed with Alcian blue destaining solution (10 % EtOH, 0.1% CH_3COOH, 0.03 M MgCl2 0.03 M in water) for 30 min at room temperature. To dissolve Alcian blue bound to the GAGs linked to the scaffolds, a solution of 1 % SDS was added in each well and left shaking (200 rpm) for 30 min. Supernatant was transferred in a new well plate and absorbance (605 nm) was read with CLARIOstar plate reader (BMG Labtech).

3.4 CELL STUDIES

Neuronal Schwann cells RT4-D6P2T (ATCC® CRL-2768™) were maintained in DMEM hight glucose (Thermo Fisher Scientific) supplemented with 2mM L-glutamine (Thermo Fisher Scientific), 10% fetal bovine serum (FBS; Sigma), and penicillin-streptomycin (100 U/mL; Sigma). Cells were removed from the culture flasks to seed the scaffolds using a trypsin-EDTA solution (Sigma). Viable cell number was determined prior to seeding by live-cell staining using 0.4% Trypan Blue (Sigma) and counting viable cells with Neubauer chamber.

The Schwann cell suspension was pipetted onto the surface of the dry scaffold (2 x 10^4 cells/well). The wells were then filled with supplemented (L-glutamine, FBS, penicillin-streptomycin) DMEM media until reach the final volume of 500 µL, placed into a cell culture incubator, and maintained at 37°C with 5.0% CO_2 for different time points (1-3-7 days).

3.4.1 CELL METABOLIC STUDIES

To measure the metabolic activity of Schwann cells seeded in scaffolds, PrestoBlue® Cell Viability Reagent (Thermo Fisher Scientific) was used. This reagent is a cell permeable resazurin-based solution that functions as a cell viability indicator by using the reducing power of living cells to quantitatively measure the metabolic activity of cells. When added to cells, the reagent is modified by the reducing environment of the viable cell and the color turns from blue to red, becoming highly fluorescent.

At the first time point (day 1), 50 µL of 9% Presto Blue in DMEM medium was added to each well as the indicator of viable cells. After an incubation at 37°C for 30 min, the solution of Presto Blue/DMEM was transferred in a new well plate to read the fluorescence using CLARIOstar plate reader.

The cell cultures were rinsed with PBS and then 500 µL of DMEM medium was added in each well. Scaffolds with cells were incubated at 37°C to repeat the metabolic assay at day 3 and 7.

3.4.2 DNA ASSAY

To determine the seeding efficiency and cell growth on the scaffolds, DNA was quantitated by using a fluorometric DNA assay on cell lysates.

At every time point, medium was removed and scaffolds with cells were rinsed with PBS, dried and transferred in new eppendorfs. Each scaffolds was frozen at −80°C for at least 24 h. Then, samples were thawed and the DNA content was measured using a CyQuant cell proliferation assay kit (Invitrogen) following the manufacturer's instructions. Samples were

incubated with 250 µL of Proteinase K (VWR) digestion buffer (1 mg/mL Proteinase K in Tris-EDTA digestion buffer) at 56°C for 16 h. Forty microlitres of sample volume were transferred into a black 96-well plate and treated with 40 µL/well RNAse for 1 h at room temperature to reassure DNA specificity. CyQuant reagent dye was added in a volume of 80 µL, incubated for 15 min protected from light at room temperature and fluorescence signals (excitation 485 nm, emission 520 nm) detected using CLARIOstar plate reader. A standard curve was performed with λDNA, provided with the kit and treated equally to the sample plates. The standard ranged from 0.5 µg/mL to 2 µg/mL λDNA and was used to calculate the final DNA content per milliliter of sample.

3.4.3 GAGs QUANTIFICATION

To measure the GAG content in the cells seeded in scaffolds a spectrophotometric assays based on 1,9-dimethylmethylene blue (DMMB) solution (38 mM DMMB, 9.5 mM HCl, 40.5 mM Glycine, 40.5 mM NaCl in water, pH 3). This DMMB solution was stable for at least 4 months when stored at room temperature in the darkness.

To extract GAGs from cells, at 1-3-7 day time points, medium was removed and scaffolds with cells were rinsed with PBS and frozen at −20°C for at least 24 h.

Samples were incubated with 250 µL of Proteinase K (VWR) digestion buffer (1 mg/mL Proteinase K in Tris-EDTA digestion buffer) at 56°C for 16 h.

Twenty five microliters of each sample were transferred into a black 96-well plate. 2.3 M NaCl (5 µL) and filtered DMMB solution (150 µL) were added in each well. The absorbance at 525 nm was directly measured using CLARIOstar plate reader. A standard curve was obtained by using a GAG standard solution (chondroitin 4- sulfate) dissolved in Proteinase K digestion buffer with 10 µg cysteine in 1 mL PBE (0,2 %). The standard ranged from 1 µg/mL to 10 µg/mL and was used to calculate the final GAG content per milliliter of sample.

3.4.4 IMMUNOSTAINING

Schwann cells cultures were fixed for 20 min with 4% paraformaldehyde at 4°C and rinsed several times with PBS. Cells were permealized with 0.1% Triton X-100 (VWR) in PBS for 15 min room temperature and then incubated in blocking solution containing 1% bovine serum albumin (BSA, VWR), 5% goat serum (Sigma) and 0.05% Tween-20 (VWR) in PBS for 1 hr. In the next step, cells were incubated with primary antibody overnight at 4°C. The primary antibodies used included rabbit antibody to laminin β2γ1 (1:250, Bioconnect), mouse antibody to integrin α9β1 (1:1000, Abcam), mouse antibody to syndecan 1 (1:1000 Abcam), and rabbit antibody to syndecan 4 (1:500, Bioconnect). Cells were washed extensively with 1% BSA, 0.05% Tween-20 in PBS and incubated in secondary antibody for 1 h at room temperature. As secondary antibodies AlexaFluor-488 goat anti-mouse, and AlexaFluor-647 goat anti-rabbit (both 1:500, Invitrogen) were used. For visualization of F-actin, cells were incubated with Phalloidin-Alexa Fluor 568 (5 µL/205 µL in washing buffer, Thermo Fisher Scientific). Nuclei were counterstained with 4,6-diamidino-2-phenylindole (DAPI) (5 min at 0.1

µg/mL, Sigma).

Cells were washed extensively with PBS and mounted in Mowiol 4-88 (Sigma) at 4°C until imaging. Samples were examined by fluorescence microscopy and images were obtained with a Nikon Eclipse Ti2 inverted microscope. Image adjustments were limited to contrast enhancement and level settings using Nikon software and Fiji (Fiji Is Just ImageJ).

3.4.5 WESTERN BLOT

At each time point, cells were placed on ice immediately following treatment and washed with ice-cold PBS. Lysis buffer included cOmplete protease inhibitor (Sigma), 2 mM Phenylmethylsulfonyl fluoride (PMSF, Sigma) and 84.7 % v/v RIPA buffer (Sigma). To minimize the presence of cells debris, protein lysate were centrifuged (10000 g) for 10 min at 4°C and supernatant was collect and stored at -80°C. For detecting Syndecan 4 neoepitopes, protein lysates were pretreated with Heparinase II (2.5 mU/µg protein, Sigma) over night at 37 °C. The protein samples were quantified with Pierce BCA protein assay kit (Thermo Fisher Scientific) and denatured with equal amount of 4X Laemmli Sample buffer (Bio-rad) with 10% 2-mercaptoethanol (Sigma) at 100°C for 5 min. For immunodetection, 10 µg of total protein from each sample was loaded and separated in 4–15% Mini-PROTEAN TGX Stain-Free Gel (Bio-Rad) and transferred by electroblotting to PVDF membranes (Bio-Rad). The membranes were blocked with 2.6 % Blocking Grade buffer (Bio-rad) in TBST (0.1% Tween-20 IN TBS) and incubated overnight at 4 °C in the same solution with rabbit antibody to laminin β2γ1 (1:250, Bioconnect), mouse antibody to integrin α9β1 (1:500, Abcam), mouse antibody to

syndecan 1 (1:250, Abcam), rabbit antibody to syndecan 4 (1:250, Bioconnect), rabbit antibody to p75 NGF receptor (1:500 Abcam), and mouse antibody to β-actin (1:2500, Sigma). Goat anti-rabbit IgG and Goat anti-mouse IgG, conjugated with horseradish peroxidase from Bio-rad (1:1500 dilution), were used as a secondary antibody. For detection, an enhanced chemiluminescence Western blot system (ECL, Bio-rad) was used. For quantification, the PVDF membranes were visualized using ChemiDoc XRS System (Bio-rad). The pictures were analyzed with software Fiji to obtain gray value of each band. Then relative gray value of each marker (gray value of special marker / gray value of β-actin) were calculated and analyzed.

3.4.6 STATISTICAL ANALYSIS

Each experiment was carried out in triplicate, except western blot (quadruplicate). All results are presented as mean – standard deviation (SD). GraphPad Prism software v 4.03 (GraphPad, San Diego, CA, USA) was used to perform the statistical analysis. Statistical significance was set at a p-value of ≤ 0.05 (*), ≤ 0.01 (**) or ≤ 0.001 (***).

4 RESULTS

4.1 ELECTROSPUN SCAFFOLDS

To determine how the rotation of a grounded mandrel affects scaffold structure, the mandrel speed has been set at 500 and 4000 RPM. Under base line conditions (mandrel RPM = 500) PCL solution produced scaffolds composed of 1.34 (± 0.23) µm diameter fibers. At 4000 RPM mandrel speed, scaffolds were made up of 1.35 (± 0.04) µm diameter fibers. In both cases nanofibers had a diameter similar to collagen fibers.

Fibers produced with different mandrel speed had a rounded cross-sectional profile and mandrel RPM did not alter average fiber diameter in scaffolds.

These data suggested that under specific conditions fiber packing is more efficient as mandrel speed was increased, a result that was consistent with the induction of increased fiber alignment. The alignment of fiber was a crucial point to mimic the pattern of some proteins like collagen and laminin in ECM during nerve regeneration. In fact, scaffolds images obtained with SEM showed that fibers obtained with a mandrel speed of 4000 RPM were aligned compared to the fibers in scaffolds produced at 200 RPM mandrel speed. As illustrated in Figure 6, directionality analysis obtained using Fiji indicated that the dispersion of fibers was obviously much more consistent in scaffolds with random fibers compared to scaffolds with aligned fibers. Effectively in this case, as shown in the graph, pixels were concentrated almost in the same direction forming a narrow peak.

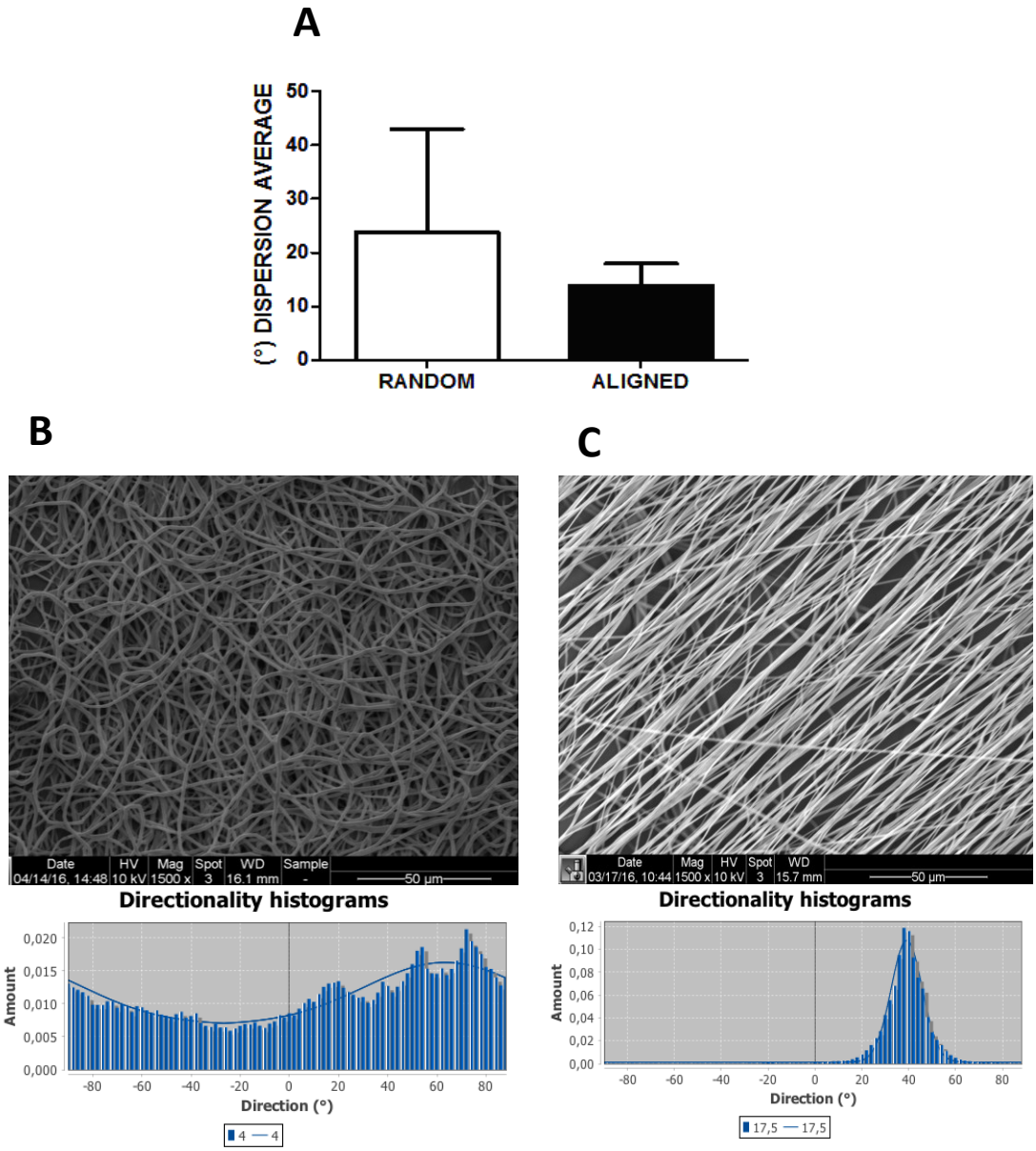

Figure 6. (A) Dispersion average of random and aligned fibers. (B) Analysis of PCL scaffolds with random fibers (mandrel speed = 500 rpm). (C) Analysis of PCL scaffolds with aligned fibers (mandrel speed = 4000 rpm).

4.2 GAGs ANALYSIS

As mentioned before, GAGs were purified from porcine vascular tissue. Quantitative analysis evidenced GAGs levels corresponding to 3.50 (± 0.08) µgUA/mg dry weight and 1.17 (± 0.03) µg UA/mg fresh weight.

Qualitative analysis showed that GAGs distribution in aortic wall followed this trend: 60% Chondroitin sulphate, 20 % Dermatan sulphate, 13% Heparan sulphate and 7% Hyaluronic Acid (Fig. 7), as reported by Naso et al. (132).

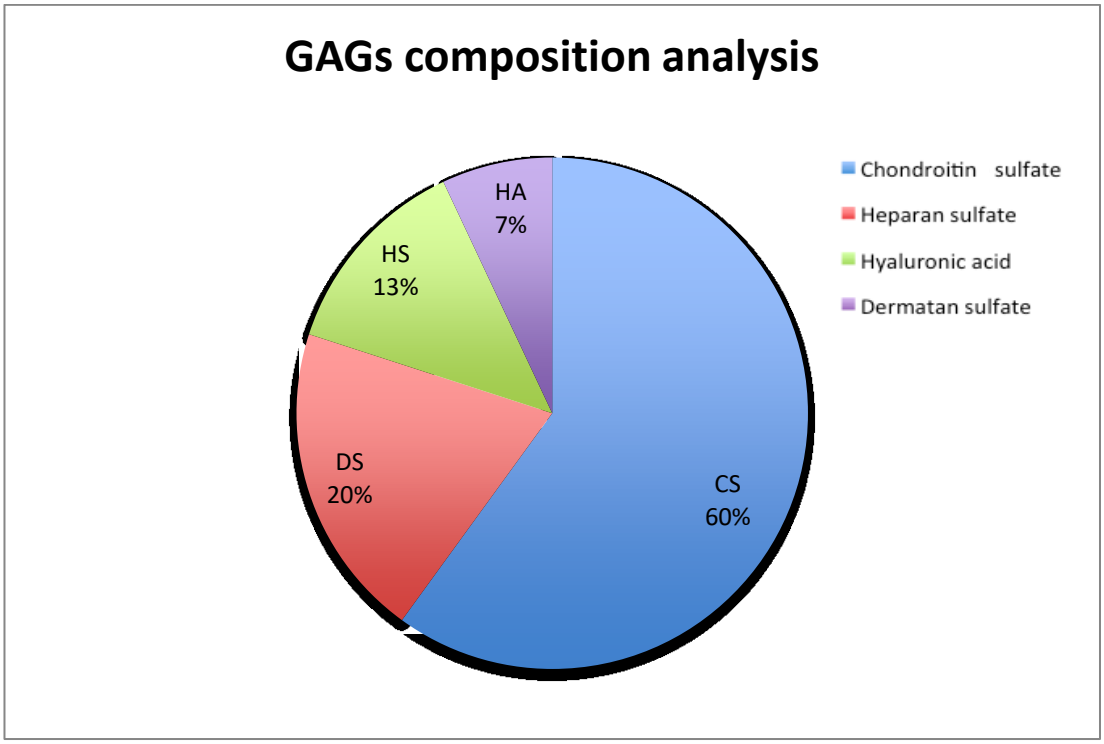

Figure 7. GAGs distribution in aortic porcine tissue.

4.3 CROSS-LINKING FUNCTIONALIZATION OF SCAFFOLDS

To evaluate if GAGs purified from aorta porcine tissue were attached to the fibers, an Alcian Blue staining protocol was developed. Scaffolds pretreated with HMDA had a percentage of GAG coating increased compared to scaffolds hydrolysed with NaOH. PCL scaffolds were activated with 1M NaOH for 30 min before the crosslinking reaction described in Materials and Methods (p. 28) (Fig. 8)

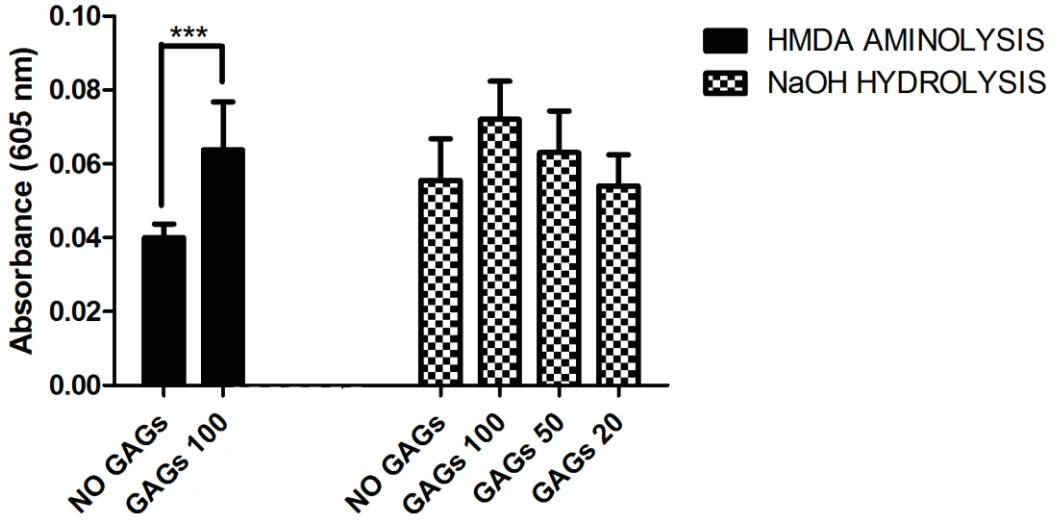

*Figure 8. Activation of functionalized PCL scaffolds. Left: scaffolds treated first with HMDA followed by a crosslinking reaction without GAGs (HMDA-EDC/NHS), and with 100 µg GAGs. Right: scaffolds activated with NaOH to generate carboxylic groups in the surface; Absorbance was read in scaffolds without GAGs (NaOH-EDC/NHS) , with 100 µg, 50 µg, 20 µg of GAGs. (***p < 0.001).*

Regarding the sterilization of scaffolds, an other experiment was set up to verify the efficiency of functionalization correlated with a step of 2h in 70% ethanol before or after crosslinking reaction (Fig. 9).

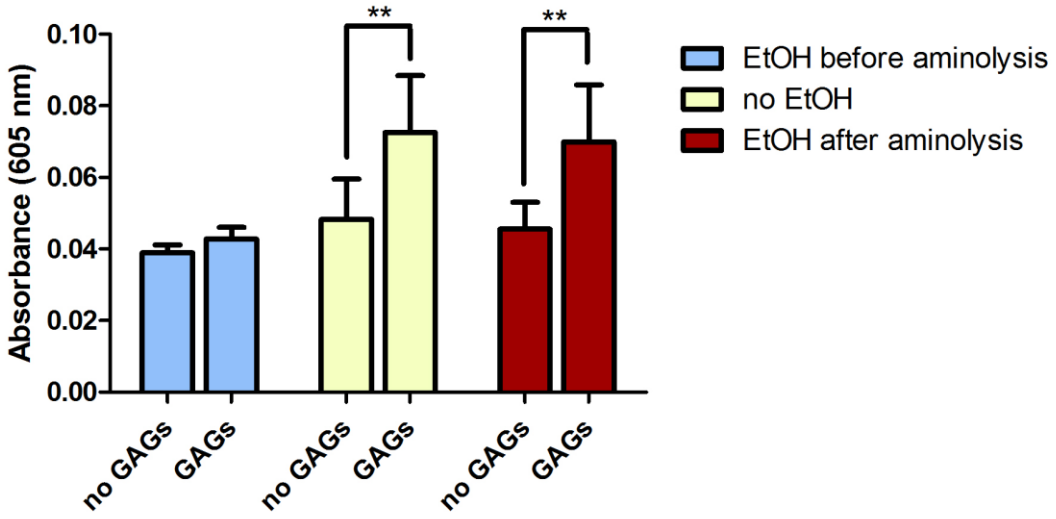

*Figure 9. Scaffolds sterilization. From left to right: scaffolds were sterilized with EtOH before functionalization with GAGs, scaffolds were functionalized without the sterilization step, scaffolds were sterilized after crosslinking reaction. The amount of GAGs used to functionalized scaffolds was 100 µg. (**p < 0.01)*

As shown in fig. 9, functionalization was more efficient when scaffolds were not sterilized, or when sterilization step was preceded by crosslinking reaction. Since aminolysis reaction takes place in isopropanol, we chose not to sterilize scaffolds so avoiding an additional step to the protocol.

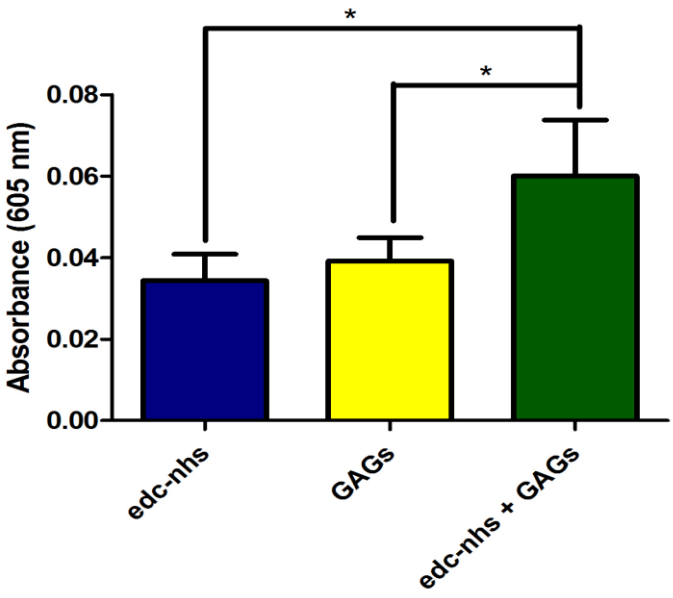

*Figure 10. PCL scaffolds functionalization through crosslinking reaction. Functionalization with EDC-NHS reagents (blue column), incubation of 100 µg GAGs (yellow column), crosslinking reaction between GAGs and PCL fibers due to EDC-NHS reagents. (*p < 0.05)*

In fig. 10 was clearly shown how functionalization of PCL scaffolds with 100 µg of GAGs through crosslinking reaction was efficient compared to functionalization with reagents but without GAGs, or functionalization with GAGs but without reagents. This result highlighted the importance of EDC-NHS reagents in crosslinking reaction. Indeed scaffolds subjected to an incubation with GAGs, showed a decrease of absorbance compared to scaffolds functionalized with the same amount of GAGs and EDC-NHS reagents.

4.4 CELL STUDIES

Preliminary results showed that in cells seeded in scaffolds both metabolic and proliferation activities, as well as GAGs production increased per time points (Fig. 11).

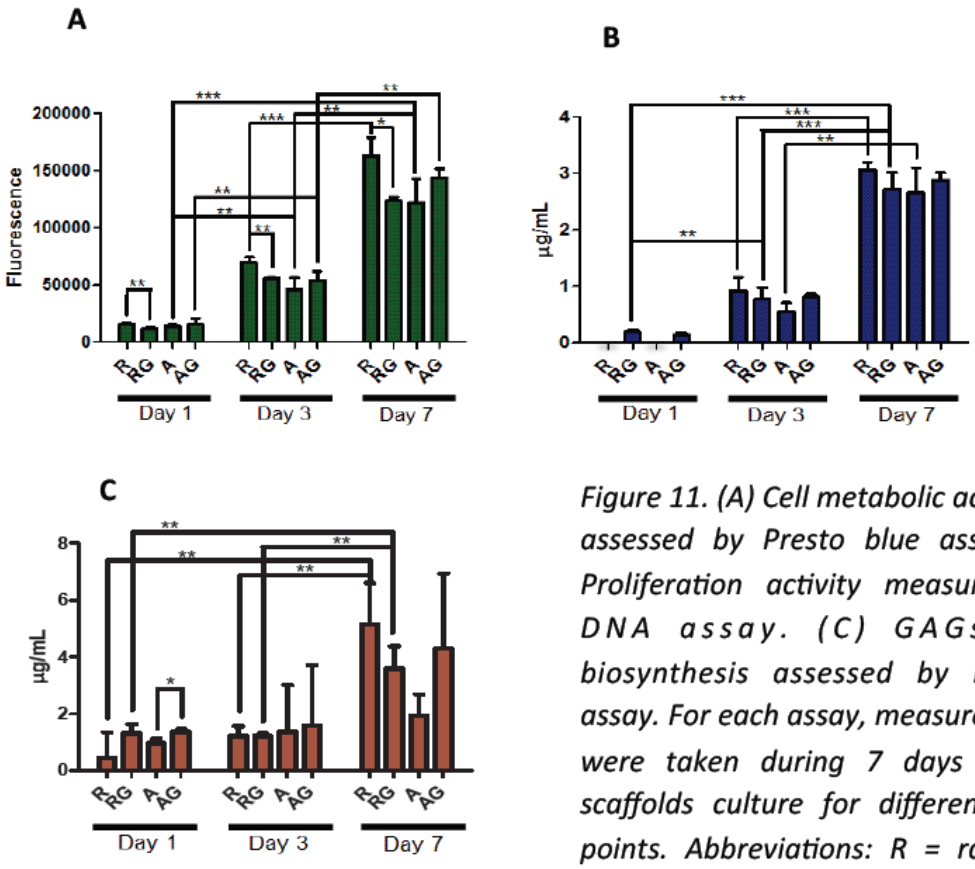

*Figure 11. (A) Cell metabolic activities assessed by Presto blue assay (B) Proliferation activity measured by DNA assay. (C) GAGs/PGs biosynthesis assessed by DMMB assay. For each assay, measurements were taken during 7 days of 3D scaffolds culture for different time points. Abbreviations: R = random, RG = random with GAGs, A = aligned, AG = aligned with GAGs. (*p < 0.05, **p < 0.01, ***p < 0.001).*

Specifically, Schwann cells showed a decrease of metabolic activities when seeded in scaffolds with random fibers functionalized with GAGs, compared to cells seeded in no functionalized scaffolds (Fig. 11, A). This phenomenon was observed at each time point (day 1-3-7). Regarding cell proliferation assay kit (Fig. 11, B), the results showed a significant increase of proliferation activities after 7 days of culture in comparison with cells at day 3 time point. Moreover, DMMB assay results showed an increase, at each time point, of sulfated GAGs in cells seeded in no functionalized and functionalized scaffolds.

Immunofluorence images showed that Schwann cells seeded in scaffolds with aligned fibers had an elongated shape which followed the direction of the fibers. On the contrary, cells seeded in scaffolds with random fibers assumed a spread structure (Fig 12).

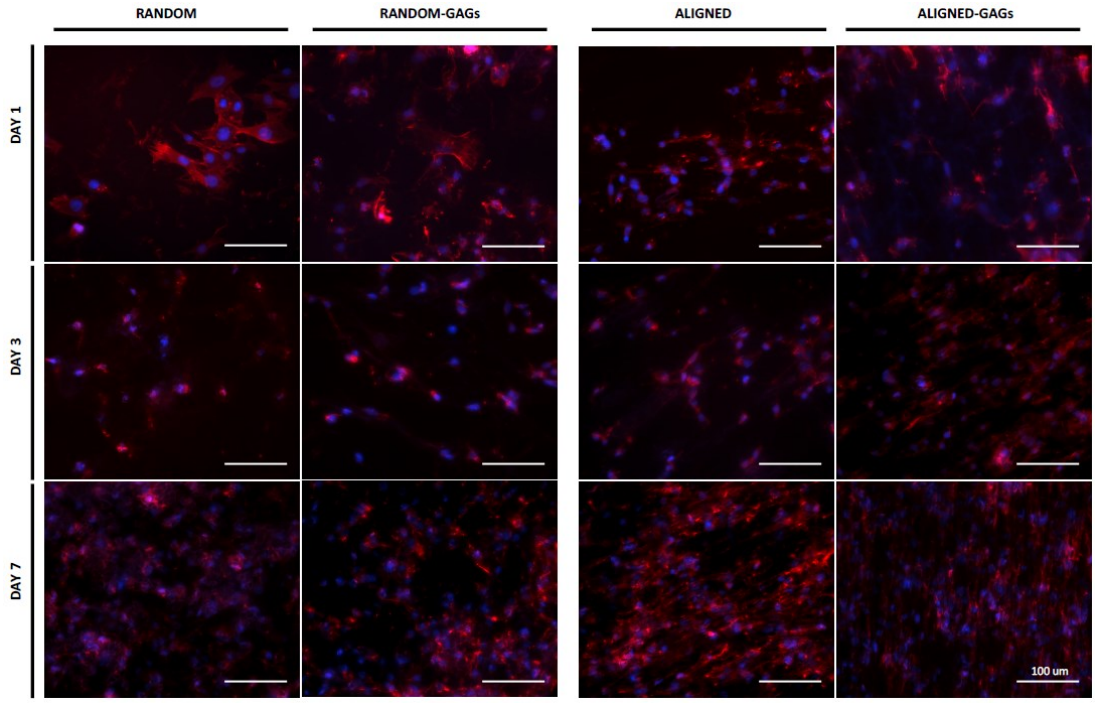

Figure 12. Immunofluorescence images. Nuclei were counterstained with DAPI. F-actin in red (Phalloidin-Alexa Fluor 568).

Since, immunofluorescence images (Fig. 14-15) showed no differences, probably for the presence of the fibers covering the cells seeded, protein expression levels were quantified by western blot assays.

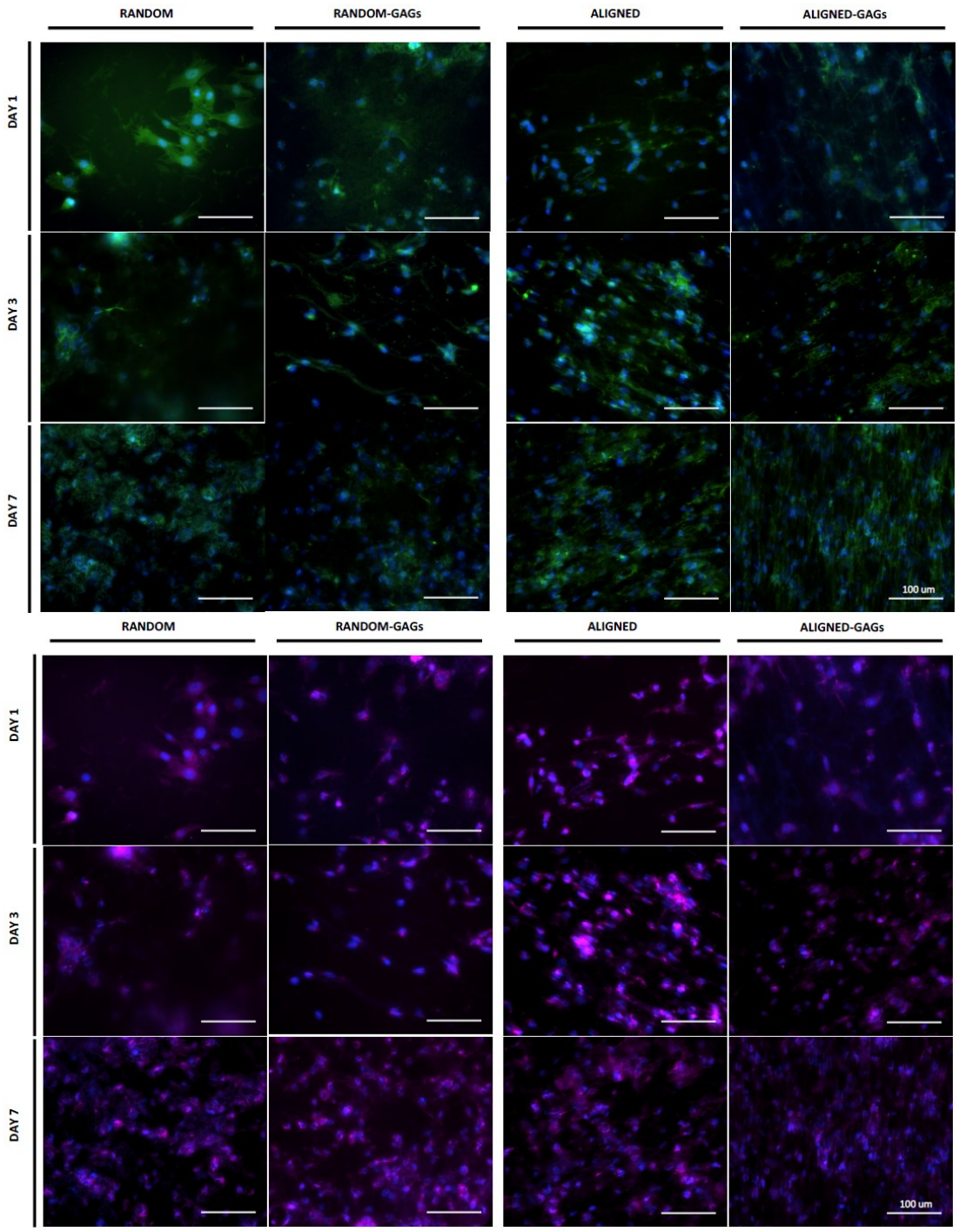

Figure 13. Immunofluorescence images. Nuclei in blue (DAPI). Upper panel: Integrin in green (AlexaFluor-488 goat anti-mouse). Lower panel: Syndecan 4 in purple (AlexaFluor-647 goat anti-rabbit).

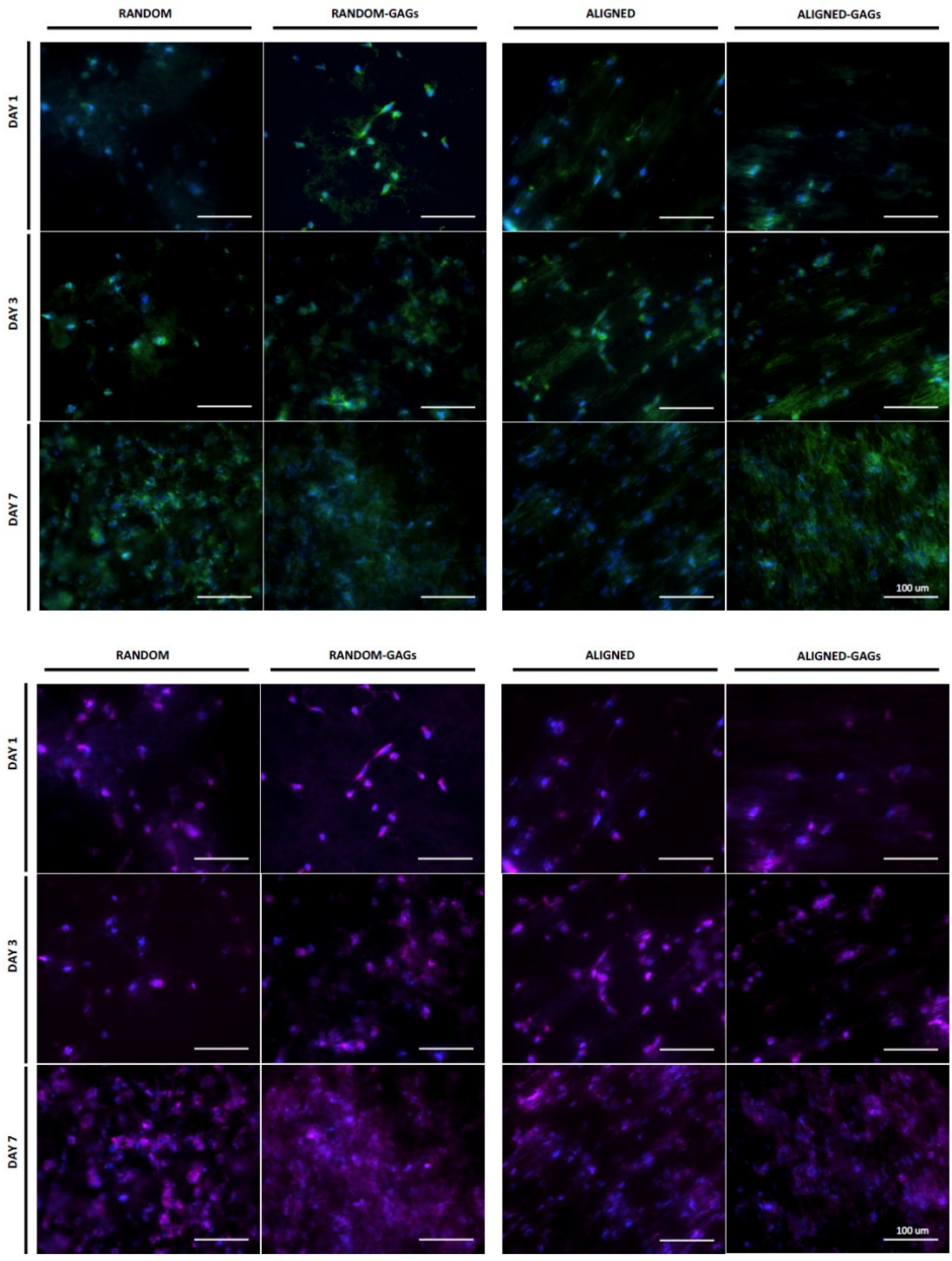

Figure 14. Immunofluorescence images. Nuclei in blue (DAPI). Upper panel: Syndecan 1 in green (AlexaFluor-488 goat anti-mouse). Lower panel: Laminin in purple (AlexaFluor-647 goat anti-rabbit).

Integrin, a transmembrane receptor involved in cell-cell and cell-matrix interactions, shows decreased levels from day 1 to day 3 and 7 (Fig. 15). This protein is known to be involved in focal adhesion in association with Syndecan 4. Interestingly, comparing the trend of protein levels between Integrin and Syndecan 4, at day 3 and 7, we observed similar patterns, probably due to their colocalization in the plasma membrane. Furthermore, at day 7, Schwann cells expressed increased Syndecan 4 levels when seeded in functionalized scaffolds with aligned fibers compared to cells seeded in no functionalized scaffolds (at the same time point) and cells seeded in functionalized scaffolds with aligned fibers at day 3.

Expression levels of Syndecan 1, a transmembrane proteoglycan implicated in the binding to ECM proteins, showed a considerable reduction from day 1 to day 3 and 7.

Laminin showed significantly decreased levels from day 1 to day 7 in cells seeded in no functionalized scaffolds with aligned fibers. However, a consistent increase of protein expression was observed in Schwann cells seeded in no functionalized scaffolds, random and aligned, after 7 days in comparison with cells at day 3. This result suggested that Schwann cells started to produce ECM proteins themselves.

A Schwann cells marker, p75 (or low-affinity nerve growth factor receptor) was detected in order to evaluate the involvement of this receptor in cells seeded in PCL scaffolds. As shown in Fig. 15, the expression levels of p75 considerably decreased from day 1 to day 3 and 7, demonstrating a similar trend with the others proteins studied.

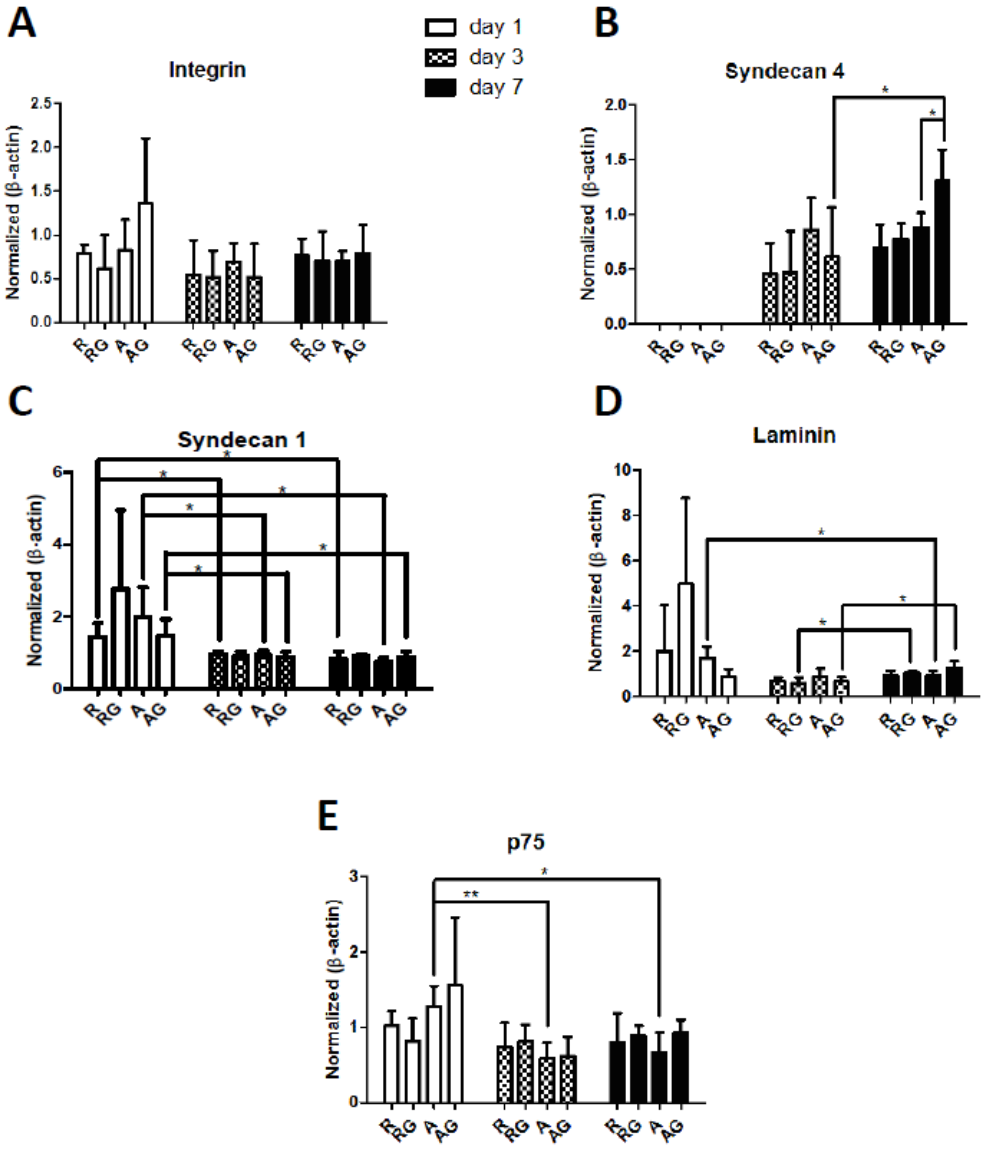

*Figure 15. Western blot analysis. (A) Integrin. (B) Syndecan 4. (C) Syndecan 1. (D) Laminin. (E) p75. All the values were normalized for β-actin. (*p < 0.05,**p < 0.01).*

One of the most important evidence is that at day 7 all the proteins studied show increased levels in cells seeded in functionalized scaffolds with aligned fibers compared to cells seeded in no functionalized scaffolds with aligned fibers. This result could be promising to improve Schwann cells proliferation in the "nerve regeneration" after traumatic nerve injury.

5 DISCUSSION

Peripheral nerve injuries (PNI) are one of the major clinical problem. In general, PNI results from motor vehicle accidents, lacerations with sharp objects, penetrating trauma (gunshot wounds) and stretching or crushing trauma, and fractures. It is estimated that PNI occur in 2.8% of trauma patients and this number reaches 5% if plexus and root lesions are included. However, due to lack of recent epidemiological studies, these data probably underestimate the actual number of nerve injuries. As mentioned above, posttraumatic nerve repair continues to be a major challenge in restorative medicine and microsurgery. Although progress has been made in surgical techniques over the last 30 years, functional recovery after a severe lesion of a major nerve trunk is often incomplete and often unsatisfactory. Functional recovery after surgical repair of mixed nerves is even more disappointing.

Compared to the central nervous system, peripheral axons have the ability to regenerate. It is known since Ramón y Cajal (1928) report that axonal elongation over long distances requires considerable assistance by Schwann cells. In neural development, axons extend to their appropriate terminal organs accompanied by Schwann cells. In axonal regeneration after a peripheral nerve injury, Schwann cells proliferate in the distal part of the transected nerve, where they form the bands of Büngner after Wallerian degeneration (136), and also stimulate the elongation of regenerating axons over longer distances by secreting neurotrophins, such as nerve growth factor (137), which are transported to the neural cell body (138).

Several animal studies have shown that prompt reinnervation of the end organ is the main determinant of a satisfactory functional recovery. It is well

known that in human clinical set there is a delay in repairing an injured nerve and this delay can cause changes that make nerve fibers unable to regenerate, and the muscles undergo atrophy and lose the ability to be reinnervated (139).Taking into account these data, researchers are constantly trying to develop strategies to increase the therapeutic success rate of regeneration and functional recovery.

Biotechnology and tissue engineering represent a multidisciplinary approach to solving some of the most demanding medical problems, particularly the creation of new tissues similar to those in the living organism. These new technical approaches include strategies in using new synthetic polymer formulations, biological constructs as well as various alternatives in tissue regeneration. Fundamental issues in tissue engineering include scaffold formation, cell cultures and cell signals.

In this PhD project, Electrospun PCL scaffolds were produced using a mandrel in which were applied two different speeds to obtain two types of scaffolds: with random fibers and with aligned fibers. The strategy was focused to mimic the pattern of some proteins like collagen and laminin in ECM during nerve regeneration. In both cases nanofibers have a diameter around 1.3 um, a fiber diameter similar to collagen fibers.

To support Schwann cells growth in a polymeric support, scaffolds were functionalized through a cross-linking reaction which allows GAGs to be bound to the fibers. The GAG molecules are long unbranched polysaccharides containing a repeating disaccharide unit. Except for hyaluronic acid, GAGs are highly negatively charged molecules, with extended conformation that imparts high viscosity to the solution in which they reside. GAGs are located primarily on the surface of cells or in the ECM but are also found in secretory

vesicles in some types of cells. However, the majority of GAGs in the body are linked to core proteins, forming proteoglycans. Many forms of proteoglycans are present in virtually all extracellular matrices of connective tissues. The major biological function of proteoglycans derives from the physicochemical characteristics of their glycosaminoglycan component, which provides hydration and swelling pressure to the tissue enabling it to withstand compressional forces. In addition to their hydrodynamic functions, proteoglycans have distinct biological functions, and their involvement in many aspects of cell and tissue activities has been demonstrated. For example, Syndecans, a family of high sulfated transmembrane proteoglycans, are implicated in the binding to ECM proteins. As a matter of fact, specific interactions between proteoglycans (through both their glycosaminoglycan and core protein moieties) and macromolecules in the extracellular matrix are key factors in the functional roles of proteoglycans.

To evaluate the role of GAGs and proteoglycans in nerve regeneration, Schwann cells were seeded in functionalized and no functionalized scaffolds with random and aligned fibers. Metabolic activity assays, proliferation assays and GAGs assays were executed. Immunofluorescence and western blot were performed using five different antibodies. Syndecan 1, a transmembrane proteoglycan, is known to be involved in cytoscheletal reorganization and in attachment of cells to ECM. On the other hand, Syndecan 4 is known to bind different proteins in ECM and also to be involved in promoting focal adhesion in co-localization with Integrins, a transmembrane receptor. In addition, we evaluated the expression levels of p75, a marker of differentiation in Schwann cells, and Laminin, an ECM protein, to observe if Schwann cells can be able to produce Laminin themselves.

Results show that in cells seeded in scaffolds both metabolic and proliferation activities, as well as GAGs production increase per time points.

Since images obtained by immunofluorescence were not very clear due to the presence of the scaffold, the levels of protein expression were evaluated by western blot assays. Except for Syndecan 4, all the proteins show a general decrease of expression level from day 1 to day 3 and day 7. Moreover at day 7 all the proteins studied reveal increased levels in cells seeded in functionalized scaffolds with aligned fibers compared to cells seeded in the same kind of scaffolds.

These results suggest that Schwann cells are metabolically active and able to proliferate in PCL electrospun scaffolds following functionalization with GAGs to create an extracellular environment similar to the natural Schwann cell basal lamina.

In conclusion, PCL–GAG scaffolds could represent a promising artificial substrate that closely mimics the recently established pattern of Schwann cells migration into the regenerating nerve.

6 REFERENCES

1. Bulow HE, Hobert O. Differential sulfations and epimerization define heparan sulfate specificity in nervous system development. Neuron. 2004;41:723-736.

2. Esko JD, Kimata K, Lindahl U: Proteoglycans and Sulfated Glycosaminoglycans. in Essentials of Glycobiology. Edited by Varki A, Cummings RD, Esko JD, Freeze HH, Stanley P, Bertozzi CR, Hart GW, Etzler ME. 2nd ed. Cold Spring Harbor (NY)2009.

3. Perrimon N, Bernfield M. Specificities of heparan sulphate proteoglycans in developmental processes. Nature. 2000;404:725-728.

4. de Wit J, Verhaagen J. Proteoglycans as modulators of axon guidance cue function. Adv Exp Med Biol. 2007;600:73-89.

5. Maeda N. Proteoglycans and neuronal migration in the cerebral cortex during development and disease. Front Neurosci. 2015;9:98.

6. Sarrazin S, Lamanna WC, Esko JD. Heparan sulfate proteoglycans. Cold Spring Harb Perspect Biol. 2011;3.

7. Kiefer MC, Stephans JC, Crawford K, Okino K, Barr PJ. Ligand-affinity cloning and structure of a cell surface heparan sulfate proteoglycan that binds basic fibroblast growth factor. Proc Natl Acad Sci U S A. 1990;87:6985-6989.

8. Mali M, Jaakkola P, Arvilommi AM, Jalkanen M. Sequence of human syndecan indicates a novel gene family of integral membrane proteoglycans. J Biol Chem. 1990;265:6884-6889.

9. Saunders S, Jalkanen M, O'Farrell S, Bernfield M. Molecular cloning of syndecan, an integral membrane proteoglycan. J Cell Biol. 1989;108:1547-1556.

10. Cizmeci-Smith G, Asundi V, Stahl RC, Teichman LJ, Chernousov M, Cowan K, Carey DJ. Regulated expression of syndecan in vascular smooth muscle cells and cloning of rat syndecan core protein cDNA. J Biol Chem. 1992;267:15729-15736.

11. Kojima T, Shworak NW, Rosenberg RD. Molecular cloning and expression of two distinct cDNA-encoding heparan sulfate proteoglycan core proteins from a rat endothelial cell line. J Biol Chem. 1992;267:4870-4877.

12. Vainio S, Jalkanen, M., Bemfield, M., and Saxen, L. Transient expression of syndecan in mesenchymal cell aggregates of the embryonic kidney. Dev Biol. 1992;152:221-232.

13. Sanderson RD, Hinkes, M.T., and Bemfield, M. (1992). Syndecan- 1, a cell-surface proteoglycan, changes in size and abundance when keratinocytes stratify. . Syndecan- 1, a cell-surface proteoglycan, changes in size and abundance when keratinocytes stratify. J Invest Dermatol. 1992; 99:390-396.

14. Yeaman C. aRA. Post-transcriptional regulation of syndecan- 1 expression by cAMP in peritoneal macrophages. J Cell Biol. 1993;122:941-950.

15. Sanderson RD, Bernfield M. Molecular polymorphism of a cell surface proteoglycan: distinct structures on simple and stratified epithelia. Proc Natl Acad Sci U S A. 1988;85:9562-9566.

16. Sutherland A.E. SRD, Mayes M., Siebert M., Calarco P.G., Bemfield M., and Damsky C.H. Expression of syndecan, a putative low affinity fibroblast growth factor receptor, in the early mouse embryo. Development. 1991;113:339-351.

17. Elenius K. VS, Laato M., Salmivirta M., Thesleff I., and Jalkanen M. Induced expression of syndecan in healing wounds. J Cell Biol. 1991;114:585-595.

18. Kim CW, Goldberger OA, Gallo RL, Bernfield M. Members of the syndecan family of heparan sulfate proteoglycans are expressed in distinct cell-, tissue-, and development-specific patterns. Mol Biol Cell. 1994;5:797-805.

19. Woods A, Couchman JR. Syndecan 4 heparan sulfate proteoglycan is a selectively enriched and widespread focal adhesion component. Mol Biol Cell. 1994;5:183-192.

20. L. WP: Gray's Anatomy. livingstone C, editor. London1999.

21. Thomas PK. The connective tissue of peripheral nerve: an electron microscope study. J Anat. 1963;97:35-44.

22. Gamble HJ, Eames RA. An Electron Microscope Study of the Connective Tissues of Human Peripheral Nerve. J Anat. 1964;98:655-663.

23. Schiff R, Rosenbluth J. Ultrastructural localization of laminin in rat sensory ganglia. J Histochem Cytochem. 1986;34:1691-1699.

24. Shanthaveerappa TR, Bourne GH. The 'perineural epithelium', a metabolically active, continuous, protoplasmic cell barrier surrounding peripheral nerve fasciculi. J Anat. 1962;96:527-537.

25. Rechthand E, Rapoport SI. Regulation of the microenvironment of peripheral nerve: role of the blood-nerve barrier. Prog Neurobiol. 1987;28:303-343.

26. Sunderland S, Bradley KC. The cross-sectional area of peripheral nerve trunks devoted to nerve fibers. Brain. 1949;72:428-449.

27. Sunderland S BK. Stress-strain phenomena in denervated peripheral nerve trunks. Brain. 1961;84:125–127.

28. Rydevik BL, Kwan MK, Myers RR, Brown RA, Triggs KJ, Woo SL, Garfin SR. An in vitro mechanical and histological study of acute stretching on rabbit tibial nerve. J Orthop Res. 1990;8:694-701.

29. Sunderland S. The anatomy and physiology of nerve injury. Muscle Nerve. 1990;13:771-784.

30. Sunderland S. The intraneural topography of the radial, median and ulnar nerves. Brain. 1945;68:243-299.

31. Millesi H, Zoch G, Reihsner R. Mechanical properties of peripheral nerves. Clin Orthop Relat Res. 1995:76-83.

32. Sunderland S. The connective tissues of peripheral nerves. Brain. 1965;88:841-854.

33. Rechthand E, Hervonen A, Sato S, Rapoport SI. Distribution of adrenergic innervation of blood vessels in peripheral nerve. Brain Res. 1986;374:185-189.

34. Appenzeller O, Dhital KK, Cowen T, Burnstock G. The nerves to blood vessels supplying blood to nerves: the innervation of vasa nervorum. Brain Res. 1984;304:383-386.

35. Burkel WE. The histological fine structure of perineurium. Anat Rec. 1967;158:177-189.

36. Bell MA, Weddell AG. A descriptive study of the blood vessels of the sciatic nerve in the rat, man and other mammals. Brain. 1984;107 (Pt 3):871-898.

37. Bell MA, Weddell AG. A morphometric study of intrafascicular vessels of mammalian sciatic nerve. Muscle Nerve. 1984;7:524-534.

38. Purves D. aNA: Trophic maintenance of synaptic connections in autonomic ganglia. in Neuronal Plasticity. Edited by Press R. C. W. Cotman Ed. ed. New York1978. pp. pp. 27–47.

39. Ducker TB, Kempe LG, Hayes GJ. The metabolic background for peripheral nerve surgery. J Neurosurg. 1969;30:270-280.

40. Lieberman AR. The axon reaction: a review of the principal features of perikaryal responses to axon injury. Int Rev Neurobiol. 1971;14:49-124.

41. Fu SY, Gordon T. The cellular and molecular basis of peripheral nerve regeneration. Mol Neurobiol. 1997;14:67-116.

42. Muller HW, Stoll G. Nerve injury and regeneration: basic insights and therapeutic interventions. Curr Opin Neurol. 1998;11:557-562.

43. Terzis J. aSK: The Peripheral Nerve. Structure, Function and Reconstruction. Press R, editor. New York1990.

44. Hokfelt T, Zhang X, Wiesenfeld-Hallin Z. Messenger plasticity in primary sensory neurons following axotomy and its functional implications. Trends Neurosci. 1994;17:22-30.

45. Fornaro M, Lee JM, Raimondo S, Nicolino S, Geuna S, Giacobini-Robecchi M. Neuronal intermediate filament expression in rat dorsal root ganglia sensory neurons: an in vivo and in vitro study. Neuroscience. 2008;153:1153-1163.

46. Tetzlaff W, Bisby MA, Kreutzberg GW. Changes in cytoskeletal proteins in the rat facial nucleus following axotomy. J Neurosci. 1988;8:3181-3189.

47. Schreyer DJ, Skene JH. Fate of GAP-43 in ascending spinal axons of DRG neurons after peripheral nerve injury: delayed accumulation and correlation with regenerative potential. J Neurosci. 1991;11:3738-3751.

48. Tetzlaff W, Alexander SW, Miller FD, Bisby MA. Response of facial and rubrospinal neurons to axotomy: changes in mRNA expression for cytoskeletal proteins and GAP-43. J Neurosci. 1991;11:2528-2544.

49. Fawcett JW, Keynes RJ. Peripheral nerve regeneration. Annu Rev Neurosci. 1990;13:43-60.

50. Mira JC. Effects of repeated denervation on muscle reinnervation. Clin Plast Surg. 1984;11:31-38.

51. Zelena J, Lubinska L, Gutmann E. Accumulation of organelles at the ends of interrupted axons. Z Zellforsch Mikrosk Anat. 1968;91:200-219.

52. Grafstein B. aMIG: Role of the nerve cell body in axonal regeneration. C. W. Cotman E, editor. New York1978.

53. S. SS: Nerves and Nerve Injuries. 2nd ed. Livingstone C, editor. Edinburgh1978.

54. Witzel C. aBT. Morphology of peripheral axon regeneration. J Peripher Nerv Syst. 2003;8:75–76.

55. Son YJ, Thompson WJ. Schwann cell processes guide regeneration of peripheral axons. Neuron. 1995;14:125-132.

56. Flores AJ, Lavernia CJ, Owens PW. Anatomy and physiology of peripheral nerve injury and repair. Am J Orthop (Belle Mead NJ). 2000;29:167-173.

57. Lubinska L. Patterns of Wallerian degeneration of myelinated fibres in short and long peripheral stumps and in isolated segments of rat phrenic nerve. Interpretation of the role of axoplasmic flow of the trophic factor. Brain Res. 1982;233:227-240.

58. Schlaepfer WW. Structural alterations of peripheral nerve induced by the calcium ionophore A23187. Brain Res. 1977;136:1-9.

59. Vial JD. The early changes in the axoplasm during wallerian degeneration. J Biophys Biochem Cytol. 1958;4:551-555.

60. Heumann R. Regulation of the synthesis of nerve growth factor. J Exp Biol. 1987;132:133-150.

61. Thoenen H, Bandtlow C, Heumann R, Lindholm D, Meyer M, Rohrer H. Nerve growth factor: cellular localization and regulation of synthesis. Cell Mol Neurobiol. 1988;8:35-40.

62. Funakoshi H, Frisen J, Barbany G, Timmusk T, Zachrisson O, Verge VM, Persson H. Differential expression of mRNAs for neurotrophins and their receptors after axotomy of the sciatic nerve. J Cell Biol. 1993;123:455-465.

63. Geuna S, Nicolino S, Raimondo S, Gambarotta G, Battiston B, Tos P, Perroteau I. Nerve regeneration along bioengineered scaffolds. Microsurgery. 2007;27:429-438.

64. Baron-Van Evercooren A, Kleinman HK, Ohno S, Marangos P, Schwartz JP, Dubois-Dalcq ME. Nerve growth factor, laminin, and fibronectin promote neurite growth in human fetal sensory ganglia cultures. J Neurosci Res. 1982;8:179-193.

65. Hall S. Axonal regeneration through acellular muscle grafts. J Anat. 1997;190 (Pt 1):57-71.

66. Liu HM. Growth factors and extracellular matrix in peripheral nerve regeneration, studied with a nerve chamber. J Peripher Nerv Syst. 1996;1:97-110.

67. Daniloff JK, Levi G, Grumet M, Rieger F, Edelman GM. Altered expression of neuronal cell adhesion molecules induced by nerve injury and repair. J Cell Biol. 1986;103:929-945.

68. Walsh FS, Doherty P. Cell adhesion molecules and neuronal regeneration. Curr Opin Cell Biol. 1996;8:707-713.

69. Aguayo AJ, Peyronnard JM, Bray GM. A quantitative ultrastructural study of regeneration from isolated proximal stumps of transected unmyelinated nerves. J Neuropathol Exp Neurol. 1973;32:256-270.

70. Sanders FK, Young JZ. The influence of peripheral connexion on the diameter of regenerating nerve fibres. J Exp Biol. 1946;22:203-212.

71. Povlsen B, Hildebrand C. Axonal regeneration in an articular branch following rat sciatic nerve lesions. J Neurol Sci. 1993;120:153-158.

72. Morris JH, Hudson AR, Weddell G. A study of degeneration and regeneration in the divided rat sciatic nerve based on electron microscopy. IV. Changes in fascicular microtopography, perineurium and endoneurial fibroblasts. Z Zellforsch Mikrosk Anat. 1972;124:165-203.

73. G. L: Nerve Injury and Repair. Elsevier, editor. Philadelphia, PA2004.

74. Salonen V, Lehto M, Vaheri A, Aro H, Peltonen J. Endoneurial fibrosis following nerve transection. An immunohistological study of collagen types and fibronectin in the rat. Acta Neuropathol. 1985;67:315-321.

75. Barton AA. An electron microscope study of degeneration and regeneration of nerve. Brain. 1962;85:799-808.

76. Thomas PK. Changes in the Endoneurial Sheaths of Peripheral Myelinated Nerve Fibres during Wallerian Degeneration. J Anat. 1964;98:175-182.

77. Bannerman PG, Mirsky R, Jessen KR, Timpl R, Duance VC. Light microscopic immunolocalization of laminin, type IV collagen, nidogen, heparan sulphate proteoglycan and fibronectin in the enteric nervous system of rat and guinea pig. J Neurocytol. 1986;15:733-743.

78. Baron-Van Evercooren A, Gansmuller A, Gumpel M, Baumann N, Kleinman HK. Schwann cell differentiation in vitro: extracellular matrix deposition and interaction. Dev Neurosci. 1986;8:182-196.

79. Bryan DJ, Litchfield CR, Manchio JV, Logvinenko T, Holway AH, Austin J, Summerhayes IC, Rieger-Christ KM. Spatiotemporal expression profiling of proteins in rat sciatic nerve regeneration using reverse phase protein arrays. Proteome Sci. 2012;10:9.

80. Brown RA, Phillips JB. Cell responses to biomimetic protein scaffolds used in tissue repair and engineering. Int Rev Cytol. 2007;262:75-150.

81. Gordon MK, Hahn RA. Collagens. Cell Tissue Res. 2010;339:247-257.

82. Durbeej M. Laminins. Cell Tissue Res. 2010;339:259-268.

83. Wallquist W, Patarroyo M, Thams S, Carlstedt T, Stark B, Cullheim S, Hammarberg H. Laminin chains in rat and human peripheral nerve: distribution and regulation during development and after axonal injury. J Comp Neurol. 2002;454:284-293.

84. Caissie R, Gingras M, Champigny MF, Berthod F. In vivo enhancement of sensory perception recovery in a tissue-engineered skin enriched with laminin. Biomaterials. 2006;27:2988-2993.

85. Wang GY, Hirai K, Shimada H, Taji S, Zhong SZ. Behavior of axons, Schwann cells and perineurial cells in nerve regeneration within transplanted nerve grafts: effects of anti-laminin and anti-fibronectin antisera. Brain Res. 1992;583:216-226.

86. Agius E, Cochard P. Comparison of neurite outgrowth induced by intact and injured sciatic nerves: a confocal and functional analysis. J Neurosci. 1998;18:328-338.

87. Singh P, Carraher C, Schwarzbauer JE. Assembly of fibronectin extracellular matrix. Annu Rev Cell Dev Biol. 2010;26:397-419.

88. Chernousov MA, Carey DJ. Schwann cell extracellular matrix molecules and their receptors. Histol Histopathol. 2000;15:593-601.

89. Hynes RO. Integrins: bidirectional, allosteric signaling machines. Cell. 2002;110:673-687.

90. Holmberg J, Durbeej M. Laminin-211 in skeletal muscle function. Cell Adh Migr. 2013;7:111-121.

91. Rudenko G, Hohenester E, Muller YA. LG/LNS domains: multiple functions -- one business end? Trends Biochem Sci. 2001;26:363-368.

92. Hormann H. Fibronectin--mediator between cells and connective tissue. Klin Wochenschr. 1982;60:1265-1277.

93. Lee HK, Seo IA, Park HK, Park YM, Ahn KJ, Yoo YH, Park HT. Nidogen is a prosurvival and promigratory factor for adult Schwann cells. J Neurochem. 2007;102:686-698.

94. Schvartz I, Seger D, Shaltiel S. Vitronectin. Int J Biochem Cell Biol. 1999;31:539-544.

95. McKee PA, Mattock P, Hill RL. Subunit structure of human fibrinogen, soluble fibrin, and cross-linked insoluble fibrin. Proc Natl Acad Sci U S A. 1970;66:738-744.

96. Mukhatyar V. KL, Yeh J. & Bellamkonda R. 2009 Tissue engineering strategies designed to realize the endogenous regenerative potential of peripheral nerves. Adv. Mat. 21, 4670 – 4679. Tissue engineering strategies designed to realize the endogenous regenerative potential of peripheral nerves. Adv Mat. 2009;21:4670 – 4679.

97. Siemionow M, Brzezicki G. Chapter 8: Current techniques and concepts in peripheral nerve repair. Int Rev Neurobiol. 2009;87:141-172.

98. Jiang X, Lim SH, Mao HQ, Chew SY. Current applications and future perspectives of artificial nerve conduits. Exp Neurol. 2010;223:86-101.

99. Madduri S, Papaloizos M, Gander B. Trophically and topographically functionalized silk fibroin nerve conduits for guided peripheral nerve regeneration. Biomaterials. 2010;31:2323-2334.

100. Siemionow M, Bozkurt M, Zor F. Regeneration and repair of peripheral nerves with different biomaterials: review. Microsurgery. 2010;30:574-588.

101. Amillo S, Yanez R, Barrios RH. Nerve regeneration in different types of grafts: experimental study in rabbits. Microsurgery. 1995;16:621-630.

102. Bertelli JA, Orsal D, Mira JC. Median nerve neurotization by peripheral nerve grafts directly implanted into the spinal cord: anatomical, behavioural and electrophysiological evidences of sensorimotor recovery. Brain Res. 1994;644:150-159.

103. Nikkhah G, Carvalho GA, Samii M. [Nerve transplantation and neurolysis of the brachial plexus after post-traumatic lesions]. Orthopade. 1997;26:612-620.

104. Bellamkonda RV. Peripheral nerve regeneration: an opinion on channels, scaffolds and anisotropy. Biomaterials. 2006;27:3515-3518.

105. Yu X, Bellamkonda RV. Tissue-engineered scaffolds are effective alternatives to autografts for bridging peripheral nerve gaps. Tissue Eng. 2003;9:421-430.

106. Trumble TE. Peripheral nerve transplantation: the effects of predegenerated grafts and immunosuppression. J Neural Transplant Plast. 1992;3:39-49.

107. Kim BS, Yoo JJ, Atala A. Peripheral nerve regeneration using acellular nerve grafts. J Biomed Mater Res A. 2004;68:201-209.

108. Krekoski CA, Neubauer D, Graham JB, Muir D. Metalloproteinase-dependent predegeneration in vitro enhances axonal regeneration within acellular peripheral nerve grafts. J Neurosci. 2002;22:10408-10415.

109. Hasan NA, Neumann MM, de Souky MA, So KF, Bedi KS. The influence of predegenerated nerve grafts on axonal regeneration from prelesioned peripheral nerves. J Anat. 1996;189 (Pt 2):293-302.

110. Jain KK. Role of nanotechnology in developing new therapies for diseases of the nervous system. Nanomedicine (Lond). 2006;1:9-12.

111. Stabenfeldt SE, Garcia AJ, LaPlaca MC. Thermoreversible laminin-functionalized hydrogel for neural tissue engineering. J Biomed Mater Res A. 2006;77:718-725.

112. Zhang L WT. Nanotechnology and nanomaterials: Promises for improved tissue regeneration. Nano Today. 2009;4:66-80.

113. Wen X, Tresco PA. Fabrication and characterization of permeable degradable poly(DL-lactide-co-glycolide) (PLGA) hollow fiber phase inversion membranes for use as nerve tract guidance channels. Biomaterials. 2006;27:3800-3809.

114. Verreck G, Chun I, Li Y, Kataria R, Zhang Q, Rosenblatt J, Decorte A, Heymans K, Adriaensen J, Bruining M, Van Remoortere M, Borghys H, Meert T, Peeters J, Brewster ME. Preparation and physicochemical characterization of biodegradable nerve guides containing the nerve growth agent sabeluzole. Biomaterials. 2005;26:1307-1315.

115. Amado S, Simoes MJ, Armada da Silva PA, Luis AL, Shirosaki Y, Lopes MA, Santos JD, Fregnan F, Gambarotta G, Raimondo S, Fornaro M, Veloso AP, Varejao AS, Mauricio AC, Geuna S. Use of hybrid chitosan membranes and N1E-115 cells for

promoting nerve regeneration in an axonotmesis rat model. Biomaterials. 2008;29:4409-4419.

116. Schmidt CE, Leach JB. Neural tissue engineering: strategies for repair and regeneration. Annu Rev Biomed Eng. 2003;5:293-347.

117. Bellamkonda R, Ranieri JP, Bouche N, Aebischer P. Hydrogel-based three-dimensional matrix for neural cells. J Biomed Mater Res. 1995;29:663-671.

118. Geller HM, Fawcett JW. Building a bridge: engineering spinal cord repair. Exp Neurol. 2002;174:125-136.

119. Carbonetto ST, Gruver MM, Turner DC. Nerve fiber growth on defined hydrogel substrates. Science. 1982;216:897-899.

120. Freed LE, Vunjak-Novakovic G, Biron RJ, Eagles DB, Lesnoy DC, Barlow SK, Langer R. Biodegradable polymer scaffolds for tissue engineering. Biotechnology (N Y). 1994;12:689-693.

121. Yang F, Murugan R, Ramakrishna S, Wang X, Ma YX, Wang S. Fabrication of nano-structured porous PLLA scaffold intended for nerve tissue engineering. Biomaterials. 2004;25:1891-1900.

122. Yang F, Murugan R, Wang S, Ramakrishna S. Electrospinning of nano/micro scale poly(L-lactic acid) aligned fibers and their potential in neural tissue engineering. Biomaterials. 2005;26:2603-2610.

123. Yang Y, De Laporte L, Rives CB, Jang JH, Lin WC, Shull KR, Shea LD. Neurotrophin releasing single and multiple lumen nerve conduits. J Control Release. 2005;104:433-446.

124. Aijun W QA, Wenling C, Mingzhi Y, Qing H, Lijun K, Ling Z, Yandao G, Xiufang Z. Porous chitosan tubular scaffolds with knitted outer wall and controllable inner structure for nerve tissue engineering. . J Biomed Mater Res 2006;79A:36-46.

125. Gibson P. S-GH, and Pentheny C. Electrospinning technology: Direct application of tailorable ultrathin membranes. J Coated Fabr. 1998; 28:63-72.

126. H. DJaRD. Electrospinning process and applications of electrospun fibers. J Electrost. 1995;35:151-160.

127. H. KJSaRD. Mechanical properties of composites using ultrafine electrospun fibers. Polym Compos. 1999;20:124-131.

128. Huang L. MRA, Apkarian R.P., Pourdeyhimi B., Conticello V.P., Chaikof E.L. Generation of synthetic elastin-mimetic small diameter fibers and fiber networks. Macromolecules. 2000;33:2989–2997.

129. Jaeger R. BM, Martin-Batille C., Schoenherr H., and Vansco G. J. Electrospinning of ultrathin polymer fibers. Macromol Symp. 1998;127:141-150.

130. K. BP. Electrostatic spinning of acrylic microfibers. J Colloid Interface Sci. 1971;36:71-79.

131. R. LLaSJM. J Polym Sci;Polym. Phys. Ed. 19:909-920.

132. Naso F, Gandaglia A, Formato M, Cigliano A, Lepedda AJ, Gerosa G, Spina M. Differential distribution of structural components and hydration in aortic and pulmonary heart valve conduits: Impact of detergent-based cell removal. Acta Biomater. 2010;6:4675-4688.

133. Cigliano A, Gandaglia A, Lepedda AJ, Zinellu E, Naso F, Gastaldello A, Aguiari P, De Muro P, Gerosa G, Spina M, Formato M. Fine structure of glycosaminoglycans from fresh and decellularized porcine cardiac valves and pericardium. Biochem Res Int. 2012;2012:979351.

134. Bitter T, Muir HM. A modified uronic acid carbazole reaction. Anal Biochem. 1962;4:330-334.

135. Cappelletti R, Del Rosso M, Chiarugi VP. A new electrophoretic method for the complete separation of all known animal glycosaminoglycans in a monodimensional run. Anal Biochem. 1979;99:311-315.

136. Reichert F, Saada A, Rotshenker S. Peripheral nerve injury induces Schwann cells to express two macrophage phenotypes: phagocytosis and the galactose-specific lectin MAC-2. J Neurosci. 1994;14:3231-3245.

137. Taniuchi M, Clark HB, Johnson EM, Jr. Induction of nerve growth factor receptor in Schwann cells after axotomy. Proc Natl Acad Sci U S A. 1986;83:4094-4098.

138. Curtis R, Adryan KM, Zhu Y, Harkness PJ, Lindsay RM, DiStefano PS. Retrograde axonal transport of ciliary neurotrophic factor is increased by peripheral nerve injury. Nature. 1993;365:253-255.

139. Martinez AM, Goulart CO, Ramalho Bdos S, Oliveira JT, Almeida FM. Neurotrauma and mesenchymal stem cells treatment: From experimental studies to clinical trials. World J Stem Cells. 2014;6:179-194.

7 COLLABORATION TO OTHER RESEARCH ACTIVITIES

In parallel with the research activity described above, I also took part in other studies that have been published in various international journals. These studies focused on evaluating potential biomarkers in pre-eclampsia as well as type I and II diabetes mellitus:

- Plasma PP13 and urinary GAGs/PGs as early markers of pre-eclampsia. *De Muro P, Capobianco G, Lepedda AJ, Nieddu G, Formato M, Tram NH, Idini M, Dessole F, Dessole S*. Arch Gynecol Obstet. 2016 Nov;294(5):959-965. Epub 2016 May 9.

- Identification of differentially expressed plasma proteins in atherosclerotic patients with type 2 diabetes. *Lepedda AJ, Lobina O, Rocchiccioli S, Nieddu G, Ucciferri N, De Muro P, Idini M, Nguyen HQ, Guarino A, Spirito R, Formato M.* J Diabetes Complications. 2016 Jul;30(5):880-6. doi: 10.1016/j.jdiacomp.2016.03.007. Epub 2016 Mar 12.

- Evaluation of Early Markers of Nephropathy in Patients with Type 2 Diabetes Mellitus. *De Muro P, Lepedda AJ, Nieddu G, Idini M, Tram Nguyen HQ, Lobina O, Fresu P, Formato M.* Biochem Res Int. 2016;2016:7497614. doi: 10.1155/2016/7497614. Epub 2016 Jan 24.